



## Supplementary Materials for

### **Adaptive introgression of a visual preference gene**

Matteo Rossi *et al.*

Corresponding authors: Matteo Rossi, [mrossi@rockefeller.edu](mailto:mrossi@rockefeller.edu); Richard M. Merrill, [merrill@bio.lmu.de](mailto:merrill@bio.lmu.de)

*Science* **383**, 1368 (2024)  
DOI: [10.1126/science.adj9201](https://doi.org/10.1126/science.adj9201)

#### **The PDF file includes:**

Materials and Methods  
Figs. S1 to S12  
Tables S1 and S2  
References

#### **Other Supplementary Material for this manuscript includes the following:**

Movie S1  
Data S1  
MDAR Reproducibility Checklist

## Materials and Methods

**Butterfly stocks.** Genetic crosses and preference trials were conducted at the Experimental Station José Celestino Mutis - Universidad del Rosario in La Vega (Colombia), between September 2019 and May 2022. Butterfly stocks for behavioral experiments were established from individuals caught around La Vega (*H. cydno cydno*; 5.0005° N, 74.3394° W) and Mocoa (*H. melpomene bellula* and *H. timareta tristero*; 1.1478° N, 76.6481° W) in Colombia, and were maintained under common garden conditions. Larvae were reared on *Passiflora oerstedii* leaves until pupation and adult butterflies were provided with ~10% sugar solution daily and *Psiguria* flowers as a source of pollen.

**Male preference trials.** We assayed preference behaviors for a total of 794 individual males across 3637 standardized choice trials (11). This included pure *H. melpomene bellula*, *H. timareta tristero*, *H. cydno cydno* males, as well as first generation (F1) *H. timareta tristero* x *H. cydno cydno* hybrids (obtained by crossing a *H. timareta tristero* male to a *H. cydno cydno* female) and backcross hybrids to *H. cydno cydno*. In brief, males were introduced into outdoor experimental cages (2x2x2m) with a virgin female of each type, either *H. cydno cydno* vs. *H. timareta tristero* females, or *H. cydno cydno* painted with a clear or red marker pen depending on the experiment (see below). 15-minute trials were divided into 1-minute intervals, where courtship (sustained hovering or chasing) was scored as having occurred or not. If a male courted the same female twice during a minute interval, it was recorded only once; if courtship continued into a second minute, it was recorded twice. Whenever possible, trials were repeated 5 times for each male. From these trials we generated a data set that includes the total number of “courtship minutes” directed toward *red* and the number of “courtship minutes” toward *white* females.

**Mimicking the *H. timareta* red forewing coloration.** In addition to experiments with *H. cydno cydno* and *H. timareta tristero* females, we recorded male preference phenotypes in trials with two artificially colored virgin *H. cydno cydno* females. One female had the dorsal side of the white forewing band painted with a red marker pen (R05, Copic Ciao, Tokyo, Japan), and the other with a transparent pen (Ciao 0, Copic Ciao) as control. These markers incorporate the same solvent (Copic Ciao, pers. communication). Unlike *H. cydno cydno* whose forewing band is white, *H. timareta tristero* has a red forewing band and this difference is determined by expression differences of the gene *optix*, which determines the placement of orange or red ommochrome pigments on *Heliconius* wings (19). Other color pattern elements also distinguish these populations, including the white hindwing margin displayed by *H. c. cydno* and a yellow hindwing bar in *H. t. tristero*. Because it is harder to match these colors across species, and because we were specifically interested in attraction to red patterns (which are the predominant difference between *H. cydno* and *H. timareta/H. melpomene* warning patterns across different geographical populations), we only manipulated the forewing in our experiments.

The red marker pen was chosen from several candidates (R14, R17, R27, R29, R35, R46 and RV29, Copic Ciao) to best mimic the forewing color of *H. timareta tristero* with regard to *Heliconius* color vision models. For this, we took photographs of red painted wings of *H. cydno cydno* and of *H. timareta tristero* with a Nikon Nikkor D7000 camera (Nikon, Melville NY, USA) with a visible light (380-750nm range allowed) and a UV (100–380 nm) filter in RAW format. A 40% gray standard was included in each photograph for color calibration. The visible light and UV images of each wing were combined to generate a multispectral image, using the “Image calibration and analysis toolbox” (47) in ImageJ (48). The reflectance spectra of the

forewing bands were extracted from the images and converted to quantum catch models (47) based on photoreceptor sensitivities of *H. erato* (49) and relative abundance of cone receptors for species in the *melpomene/cydno* group (49) (*H. erato* was the only *Heliconius* species for which photoreceptor cell sensitivities had been reported at the time of this analysis). Note that *Heliconius* can discriminate in the red-range even though they have only one long-wavelength (LW) opsin with peak sensitivity at 560nm due to the presence of red-filtering pigments in some ommatidia (50), that shifts the peak absorbance of some cones to ~600nm (51). However, this was not modeled in a first instance because the relative abundance of this cone receptor remains unknown (but see below).

We initially calculated pairwise “just noticeable differences” (JND) using a tetrachromatic (*H. erato*) color vision model with noise-limited opponent color channels, after (52), between the forewing band of *H. timareta tristero* and the red-painted *H. c. cydno* band using a Weber fraction of 0.05. The marker R05 had the lowest pairwise JND (0.89) and was therefore the marker we used to manipulate the forewing colors in experimental *H. cydno* females. A JND value less than 1 is considered to be generally indistinguishable by visual systems (53). To further corroborate that *Heliconius* males perceive the artificial and natural red patterns similarly, we acquired reflectance spectra of the artificial (red and clear) and natural (red and white) pattern elements using an Ocean Optics FLAME-T-XR1-ES spectrometer, a UV/Vis bifurcated fiber and a PX-2 Pulsed Xenon Lamp. A spectralon white standard (Ocean Optics WS-1) was used to calibrate the spectrometer. Each color pattern (i.e., the forewing bar) was measured at three different locations (using an average of three scans), and the mean of the three measurements was used for further analyses. The reflectance data was analyzed through a tetrachromatic color vision model incorporating more recently published *H. melpomene* photoreceptor cell sensitivities (54). This differs from the model above in that we removed one UV channel and added the chromatic channel (red-shifted;  $\lambda_{\max} = 590$ ) linked to the presence of red filtering pigments (54) (UV-Rhodopsin1 ( $\lambda_{\max} = 360$  nm), blue-Rhodopsin ( $\lambda_{\max} = 470$ nm), long wavelength-Rhodopsin without filtering pigments ( $\lambda_{\max} = 570$ nm)). Photoreceptor cell abundances are not available for this newly classified photoreceptor type so we were unable to calculate JND values. Nevertheless, the reflectance spectra of the artificial and natural patterns overlap in shape and in tetrahedral color space when viewed under standard daylight (illum = "D65") against green foliage (bkg = "green") and with von Kris color correction (vonkries = TRUE; Figs. S1A and S1B respectively).

Genotyping of backcross hybrids. Genotypes at the QTL peak (i.e., the region of strongest statistical association) for variation in preference behavior between *H. cydno* and *H. melpomene* on chromosome 18 (11) segregates with the presence of the red forewing band in our crosses due to tight linkage with the major color pattern gene *optix*. Because the presence of the red band is dominant over its absence, we were able to infer genotype at the *optix* locus by inspecting the forewing band color in backcross to *H. cydno* hybrids (26). Specifically, hybrid individuals with a red band are heterozygous for *H. timareta*/*H. cydno* alleles, and individuals lacking it are homozygous for the *H. cydno* allele. This allows a conservative test of whether this genomic region at the end of chromosome 18 influences variation in male preference based on wing pattern phenotype alone (26). Nevertheless, to confirm the segregation of *optix* alleles with red-color pattern in hybrid crosses and assay more specifically the genotype of hybrids at tightly linked candidate genes in the QTL peak on chromosome 18, we performed PCR amplification of a *regucalcin1* segment (found within the QTL peak). Analysis of whole genome sequence data

(see below) identified indels differentiating *H. timareta* and *H. cydno* in this region, so we designed primers to encompass these putative indels at the level of *regucalcin1* (Table S2A). Genomic DNA (gDNA) was extracted from thorax tissue of our cross (*H. cydno cydno* and *H. timareta tristero*) grandparents, (*H. cydno cydno* and F1) parents and backcross hybrid progeny, using a DNAeasy Blood & Tissue kit with RNase A treatment (Qiagen, Valencia, CA, USA). Samples had previously been stored in 20 % DMSO, 0.5 M EDTA (pH 8.0) solution. We found that *H. cydno* and *H. timareta* individuals consistently differed in size of the PCR-amplified fragment, allowing us to infer genotype in the hybrid progeny. Similarly, we found indels that differentiate the two species within the QTL peak on chromosome 1 allowing us to infer genotype at this chromosomal location as well (Table S2A).

Behavioral data analysis. We fitted generalized linear mixed models (GLMM) with binomial error structure and logit link function implemented with the R package lme4 to test for the effect of species or genotype on male preference. Specifically, we modeled the response vector of the number of “courtship minutes” toward the ‘red’ female (i.e., the *H. timareta tristero* or a red painted *H. cydno cydno* female) versus “courtship minutes” toward the ‘white’ (i.e., the *H. cydno cydno* or transparent painted *H. cydno cydno* female) and included type (i.e., species or genotype) as fixed factors. Significance was then determined by comparing models with type included as a fixed factor to models in which it was removed using likelihood ratio tests. An individual level random factor was included in all models to account for overdispersion, e.g., (55). Estimated marginal means and their confidence interval were extracted with the R package emmeans.

For our analysis testing the effect of genotype at the end of chromosome 18 on preference towards *H. timareta tristero* vs. *H. cydno cydno* females, we used the full data set of all 157 backcross males that courted *H. timareta* or *H. cydno* at least once during the trials. Genotype was initially determined from forewing color, but we updated this for 3 males of 130 males successfully genotyped at *regucalcin1* (found within the QTL peak), where we detected recombination between *regucalcin1* and *optix* (i.e., *optix cydno-cydno* – white forewing, QTL peak/*regucalcin1 timareta-cydno*). We note that any recombination between these loci in the individuals that we were unable to successfully genotype at *regucalcin1* will be rare (we expect just 0.62 recombination events between these two loci across the remaining 27 individuals that we could not genotype).

Although we were primarily interested in the effect of the QTL on chromosome 18, which has explicitly been shown to influence differences in visual preference between *H. cydno* and *H. melpomene* (11), two additional QTL have been implicated in variation in male mating preference between *H. cydno* and *H. melpomene* (11). The associated 1.5 lod confidence region of one of these incorporates the whole of chromosome 17, and in general is less well supported (11, 27). However, another behavioral QTL can be localized to a specific region of chromosome 1, for which we were able to generate genotypes (see above). To additionally include this in our analysis, we repeated our analysis of the backcross hybrids, but this time using a reduced data set including only individuals that we were able to genotype successfully at previously identified QTL on chromosome 1 and 18 (see above for details). This time the model included two fixed factors (genotype at the chromosome 18 QTL, and genotype at the chromosome 1 QTL); significance was determined by dropping each in turn and once again assessed with likelihood ratio tests. There were no quantitative differences from our previous analysis for the QTL on chromosome 18. In contrast, there was only very limited support that the QTL on chromosome 1

influences preference differences between *H. timareta* and *H. cydno* ( $n=128$ ,  $2\Delta\ln L = 3.79$ ,  $P = 0.0515$ ), and as such we did not include this QTL in subsequent analysis. Finally, in our analysis considering preference by backcross hybrids towards red and transparent colored *H. cydno* females, we again used forewing color to determine genotype at the end of chromosome 18.

gDNA extraction and whole-genome resequencing. gDNA was extracted from thorax tissue of 4 *H. melpomene bellula* and 11 *H. t timareta tristero* individuals as well as the parents of F1 hybrids (2 *H. t timareta tristero*, 2 *H. cydno cydno*, 2 *H. melpomene rosina*, 2 *H. cydno chioneus*, see below), that were previously stored in 20 % DMSO, 0.5 M EDTA (pH 8.0) solution, using a DNAeasy Blood & Tissue kit, with RNase treatment (Qiagen). Illumina whole-genome resequencing libraries were prepared and sequenced at Novogene (Hong Kong, China) in 125bp or 150bp paired-end mode (two different batches for *H. timareta tristero* individuals, respectively 9 and 2 samples). Previously compiled and published whole-genome resequencing data were retrieved for 5 *Heliconius numata*, 4 *H. melpomene bellula*, 10 *H. cydno chioneus*, 10 *H. cydno zelinde*, 10 *H. melpomene rosina*, 10 *H. melpomene amaryllis* and 10 *H. timareta thelxinoe* (31, 56–58). Whole-genome resequencing reads were mapped to the *H. melpomene* genome version 2 (59) with BWA mem v.0.7.15 (60). Duplicate reads were marked with Picard (<https://broadinstitute.github.io/picard/>) and variant calling was performed with GATK v3.7 HaplotypeCaller (61) with default parameters except heterozygosity set to 0.02 (parameters as in (31), for comparable analyses). Individual genomic records were combined and jointly genotyped (GATK's GenotypeGVCFs) for each subspecies.

Admixture proportions,  $F_{ST}$  and  $d_{xy}$  calculation. We calculated  $f_d$  (29), an estimate of admixture proportion based on the ABBA-BABA test, between *H. melpomene* and *H. timareta* populations as in (31) and implementing scripts available at <https://github.com/simonhmartin/>. For this, variant sites had to be biallelic SNPs (no indels), with Genotype Quality (Q) >30 and read depth (DP) >8. In addition, variant sites were filtered out if > 30% of individuals had missing genotype calls and if > 75% of individuals had heterozygous calls. The following populations were used to estimate admixture proportions: *H. cydno chioneus* and *H. cydno zelinde* as a (combined) allopatric control population, *H. timareta tristero* and *H. melpomene bellula* (or, in a separate analysis, *H. timareta thelxinoe* and *H. m. amaryllis*) as the two sympatric species, and *H. numata bicoloratus* as the outgroup.  $f_d$  was calculated in 20kb sliding windows (step = 5kb). For  $f_d$  estimates, only sites where >60% of individuals had a genotype were considered and  $f_d$  values had to be based on  $\geq 300$  ABBA-BABA informative sites per window. We also calculated sequence divergence ( $d_{xy}$ ) (62) and the fixation index ( $F_{ST}$ ) (63) in sliding 20kb windows (step = 5kb, 2000 genotyped sites required per window) with the script 'popgenWindows.py' available at <https://github.com/simonhmartin/>.

Topology weighting. To quantify phylogenetic relationships between species in genomic intervals along the QTL region associated with visual preferences, we used *Twisst* (32). We used the same invariant/variant sites filtered as above (for  $f_d$  estimation), with the further requirement that at each site no more than 25% of individuals were permitted missing genotypes. Genotypes were phased and imputed using Beagle (64). Neighbor-joining trees (65) were inferred using PhyML (66)(substitution model = GTR), as implemented in *Twisst*. Weightings for 15 possible topologies (rooted with *H. numata* as the outgroup) were estimated for non-overlapping 50 SNPs windows.

Linkage disequilibrium. If divergent male preferences lead to divergent patterns of mating a positive genetic correlation may be expected to build up between signal and preference loci (8, 33). To test this, we calculated linkage disequilibrium (LD) patterns by using whole-genome resequencing data of 10 *H. melpomene rosina* and 10 *H. cydno chioneus* and 9 *H. timareta tristero* and 9 *H. cydno cydno*. Genotypes were called using the genome analysis tool kit (GATK) Haplotypecaller as above. Variant genotype calls were filtered to a minimum depth (DP)  $\geq 10$ , and a minimum genotype quality (GQ)  $\geq 30$ . We used Beagle v5.4 to phase genotypes using default settings (67). LD between pairs of SNPs was calculated using the VCFtools (68) option `-hap-r2` with a minor allele frequency of 0.2 and a thinning distance of 1,000 bp. Kernel densities of  $R^2$  values larger than 0.8 were visualized using the `kde2d` function of the R package MASS (69), using a bandwidth ( $h$ ) of 200,000 and 500 grid points ( $n$ ).

Selective sweeps. To determine whether the regions we detected with our admixture proportion and topology weighting analyses are under selection, suggesting *adaptive* introgression, we tested for evidence of selective sweeps across the QTL region. Variant sites were filtered for genotype quality (GQ)  $> 30$  and read depth (DP)  $> 10$ , and required to be biallelic SNPs (no indels). Furthermore, variant sites had to be called in 8 individuals out of 10 for the focal population, and in 3 individuals out of 5 for the outgroup. Sites were polarized (ancestral vs. derived) using *H. numata* as an outgroup. The background site-frequency-spectrum (SFS) was computed across the whole-genome with the exception of the Z chromosome. We used SweepFinder2 (34), which has been previously used to detect introgressed sweeps at color pattern loci in *Heliconius* (70), to estimate the composite likelihood ratio (CLR) of a sweep model compared to a neutral model (neutrality is represented by the background SFS of the genome) in 50bp steps, using both polymorphic sites and substitutions (71). We considered those regions with top 1% quantile CLR values as having undergone a putative selective sweep.

Brain tissue collection, RNA extraction and sequencing. Brain (optic lobes and central brain) and eye (ommatidia) tissue were dissected out of the head capsule (as a single combined tissue) of sexually naive, 10-days old males, in cold (4 °C) 0.01M PBS. *Heliconius* males don not start courting females until they are mature (normally ~five days)(72), so by sampling males at ten days post-eclosion we could ensure that they were sexually mature, as well as controlling for age. We decided to direct our sampling efforts on males in order to maximize the number of biological replicates across populations with different preference phenotypes. We sampled a total of 5 *H. melpomene bellula*, 5 *H. melpomene melpomene*, 5 *H. timareta tristero*, 4 *H. cydno cydno*, and 4 F1 hybrids *H. cydno cydno* x *H. timareta tristero*, which were stored in RNAlater (Thermo Fisher, Waltham, MA, USA) at 4 °C for 24 hours, and subsequently at -20 °C until RNA extraction. Previously compiled RNA-seq data for 5 *H. melpomene rosina*, 5 *H. cydno chioneus*, 6 F1 hybrids *H. melpomene rosina* x *H. cydno chioneus* (generated with the same methods/in the same sequencing batch) were retrieved from (27). A further 5 *H. m. amaryllis* males were sampled from outbred stocks maintained at the Smithsonian insectaries in Gamboa, Panama. RNA was extracted and purified using TRIzol Reagent (Thermo Fisher) and a PureLink RNA Mini Kit with PureLink DNase digestion on column (Thermo Fisher). Illumina 150bp paired-end RNA-seq libraries were prepared and sequenced (in a single batch) at Novogene.

Differential gene expression and exon usage. After trimming adaptor and low-quality bases from raw reads using TrimGalore v.0.4.4 ([www.bioinformatics.babraham.ac.uk/projects](http://www.bioinformatics.babraham.ac.uk/projects)), RNA-seq

reads were mapped to the *H. melpomene* v. 2 genome (59)/ *H. melpomene* v. 2.5 annotation (73) using STAR v.2.4.2a in 2-pass mode (74) with default parameters (at first, see below). Only reads that mapped in ‘proper pairs’ were kept for further analysis using Samtools (75). For gene expression analyses, the number of reads mapping to each annotated gene was estimated with HTseq v. 0.9.1 (model = union) (76). For exon usage analyses, the number of reads mapping to each annotated exon was estimated using the python script “dexseq\_counts.py” from the DEXSeq package (76). Differential gene expression analyses were conducted with DESeq2 (77), differential exon usage analyses with DEXSeq (76). Pairwise transcriptomic comparisons were conducted only between species raised in the same insectary locations (either Panama or Colombia) to avoid the confounding effect of environmentally-induced gene expression changes (Fig. S5). To account for differences in tissue composition, we considered only those genes showing a 2-fold change in expression level at adjusted (false discovery rate 5%) p-values < 0.05 (Wald test) to be differentially expressed (78).

An initial finding that all red-preferring subspecies showed a significantly higher expression of the last exon (i.e. exon 5) of *regucalcin1* (HMEL013551g4) compared to white preferring species, prompted us to study whether the highly divergent sequence of red-preferring (including the *H. melpomene* reference genome) vs. white-preferring subspecies in this region might have affected this. In fact, when using more permissive parameters than the default parameters in STAR v.2.4.2a (see below), differential usage of exon 5 of *regucalcin1* disappeared in many comparisons. Given that i) with these permissive parameters there is uniform RNA-seq reads coverage of exon 5 in *H. cydno* subspecies ii) when using even more permissive parameters (parameters set 2, see below) the results remain unchanged, and that iii) when using ISO-Seq data from *H. cydno* to assemble the *regucalcin1* transcript, exon 5 is included (see below), we concluded that the more permissive parameters are more appropriate, and that, the initial finding of consistent differential exon 5 usage is likely an artifact of too stringent (default) mapping parameters. We find no consistent significant changes in exon usage across all comparisons with these new parameters.

RNA-seq mapping parameters. The default mapping parameters in STAR v.2.4.2a (63) were changed to more permissive ones (parameters set 1):

```
--outFilterMismatchNmax 15 --outFilterMismatchNoverReadLmax 0.1 --  
outFilterMismatchNoverLmax 0.1 --outFilterScoreMinOverLread 0.5 --  
outFilterMatchNminOverLread 0.5.
```

We also conducted the same analyses with yet more permissive parameters (parameters set 2):

```
--outFilterMismatchNmax 20 --outFilterMismatchNoverReadLmax 2 --  
outFilterMismatchNoverLmax 0.2 --outFilterScoreMinOverLread 0.33 --  
outFilterMatchNminOverLread 0.33.
```

PacBio isoform sequencing. Brain (optic lobes and central brain) and eye (ommatidia) tissue were dissected out of the head capsule (as a single combined tissue) of sexually naive, 10-days old males, in cold (4 °C) 0.01M PBS. Tissues were stored in RNAlater (Thermo Fisher, Waltham, MA, USA) at 4 °C for 24 hours, and subsequently at -20 °C (Colombian samples) or -80 °C (Panamanian samples) until RNA extraction. RNA was extracted and purified using TRIzol Reagent and a PureLink RNA Mini Kit with PureLink DNase digestion on column from a pull of whole-brain and eye tissue of the same subspecies (4 *H. melpomene rosina*, 4 *H. timareta tristero* and 2 *H. cydno chioneus* male individuals) for a total of 3 libraries, one for each

subspecies. Single molecule real-time (SMRTbell) libraries were prepared and sequenced at Novogene (Hong Kong, China), on a PacBio RSII platform (Pacific Biosciences, Menlo Park, CA, USA).

Isoform assembly/discovery and transcript-guided annotation. Following the custom IsoSeq v3 pipeline (<https://github.com/PacificBiosciences/IsoSeq/>), Iso-Seq subreads from each library were used to generate circular consensus sequences (ccs), and polyA tails and artificial concatemers were removed (primers = 5' AAGCAGTGGTATCAACGCAGAGTACATGGG, 3' GTACTCTGCGTTGATACCACTGCTT). Bam files were transformed into fastq format using Samtools (75). Reads were mapped to the *H. melpomene* 2 (59) genome using *minimap2* (79) with default parameters for PacBio Iso-Seq (-ax splice:hq). Stringtie2 (80) was used to assemble de-novo transcripts, in order to conduct between-species comparison of isoform expression. However, coverage of Iso-Seq reads was low and the resulting transcriptome annotation sparse/incomplete not permitting inference of differential isoform expression between species.

Allele-specific expression (ASE) analyses. 8 parental individuals of the F1 hybrids *H. melpomene rosina* x *H. cydno chioneus* and F1 hybrids *H. cydno cydno* x *H. timareta tristero* (two broods for each F1 hybrid type), were genotyped using GATK v3.7 HaplotypeCaller. Individual genomic records were filtered with “hard-filters” following the GATK’s Best Practices. From these filtered variants, we extracted variant sites with opposite alleles between each parental pair with *bcftools intersect*. At the same time, we marked duplicate F1 hybrid RNA-seq reads with Picard v.1.8 (<https://broadinstitute.github.io/picard/>), applied the GATK’s SplitNCigarReads function and genotyped RNA-reads with HaplotypeCaller. We filtered out variant sites from F1 hybrid RNA-seq reads that had quality by depth (QD) < 2 and strand bias (FS) >30, and kept only biallelic heterozygous SNPs for further analysis (allele-informative sites should be heterozygous for the parental alleles).

Finally, we used GATK’s ASEReadCounter (without deduplicating RNA reads) to count how many RNA-reads mapped to either parental allele. We tested for differential allele specific expression for each gene with the model “~0 + individual + allele” in DESeq2 (setting sizeFactors = 1, i.e., without library size normalization between samples). By testing for ASE in F1 hybrids we can also confirm that known volumetric differences between *H. melpomene* and *H. cydno/H. timareta* (42) do not account for differences in *regucalcin1* gene expression.

Immunocytochemistry. Two affinity-purified polyclonal rabbit antibodies against *regucalcin1* were developed with a *ThermoFisher* 70-days immunization protocol. Criterion to avoid cross-interaction with other epitopes was that less than 4 amino acids matched with another predicted protein from the *H. melpomene* genome assembly/annotation (Hmel2.5) (52, 62). The antigen target region is "EPGKFHLKKGALYRIDED". Antibodies were stored at -20°C in 50% glycerol.

Heads of insectary-reared *H. melpomene rosina* male individuals of 2-8 days of age were fixed in paraformaldehyde (PFA) 4% for 24 hours. Brains were dissected out of the head capsule in 0.02M PBS, removing the ommatidial, retinal and laminal tissue, and then embedded in 4% agar and sliced at 100µm with a LeicaVT1200S vibratome. In a first set of experiments, eyes were not included in the preparation. Brain sections were washed with blocking solution (BS: 1% Triton X-100 ; 0.1% Saponin; 1% bovine serum albumin) 3 times for 60 minutes at room temperature and then incubated at 4°C for 2 days with 1:100 rabbit *regucalcin1* primary antibody (we combined an equal amount of two immunized rabbits sera, with 1.24 and 2.5 mg/ml

concentration respectively before glycerol dilution) and 1:30 mouse *synapsin* primary antibody to stain for neuropil (anti SYNORF1, Developmental Studies Hybridoma Bank, University of Iowa, Iowa City, IA, RRID: AB\_528479) in BS solution. Samples were washed 3x30min in BS at room temperature, and then incubated for 1 day at 4°C with Alexa 647 anti-rabbit (Dianova, 711-606-152, 1:300), Cy3 anti-mouse (Dianova 715-166-151, 1:400), and Neuro Trace blue (Mol probes invitrogen, 1:300) in BS. Finally, samples were washed 3x30min in PBS, and then mounted in Vectashield medium.

Samples including eyes were subsequently fixed as above and sliced at 100µm. We performed three controls on a different set of butterflies to confirm the specificity of antibodies incubating these tissue slices in: i) only 1:100 rabbit *regucalcin1* primary antibody mixture; ii) only secondary Alexa 647 anti-rabbit without previous incubation with primary antibodies; and iii) 1:100 rabbit *regucalcin1* primary antibodies and 50x excess blocking peptide (1:50 antibody to peptide used in the immunization protocol), that had been pre-incubated together at room temperature for 2 hours in BS, followed by an incubation with Alexa 647 anti-rabbit secondary antibody. In these experiments, Neuro Trace blue was used as counterstain. Samples were incubated and washed as stated in procedures above for one night (primaries) and one night (secondaries).

Western blot. We ran a Western blot to confirm that our antibody binds to a protein of predicted size for *regucalcin1*. Whole *H. melpomene* brain tissue was lysed in 100ul of 1xLaemmli buffer (1x 60 mM Tris/HCl pH 6.8, 2% SDS, 8% Glycerol, 2.5% β-Mercaptoethanol, 0.0025% Bromphenol Blue). Samples were boiled for 5 minutes at 95°C, prior to loading on a 10% SDS gel. Gels were run at 80V for 10 minutes and 130V for 80 minutes. After semi-dry blotting for 90 minutes under constant current of 256mA, the PVDF (VWR #10600021) membranes were blocked in 5% (w/v) dry milk in 1x PBS at 4°C overnight. Next, primary antibody incubation was also performed overnight at 4°C, followed by 3x10 minutes washing with 1xTBS, and then 1-hour incubation with HRP-conjugated secondary antibodies, both at room temperature. After washing with 1xTBS (3x10 minutes), detection was done based on enhanced-chemiluminescence (using BIO-RAD reagents #1705062S), and protein masses were estimated using the Blue Prestained Protein Standard (NEB #P7718). We used rabbit anti-*regucalcin1* antibody as above (1:100, combining an equal amount of the two purified antibodies), for detection of *regucalcin1*; and rabbit anti-*regucalcin1* (1:100) + blocking peptide (1:50), as negative control. For the latter, rabbit anti-*regucalcin1* (1:100) was first incubated for 3 hours at room temperature with 1:50 Peptide, before incubation with the membrane.

Confocal imaging and image analysis. Brains were imaged with a Stellaris 5 confocal microscope (Leica) equipped with a white light laser and a 405nm laser, and a HC PL APO CS2 40x /1.10 water immersion objective and with the tile scanning function. Excitation wavelengths and emission filters were 405 nm and 476-549 nm for neurotrace blue, 554 nm and 559-658 nm for Cy3, and 653nm and 658-750 nm for Alexa 647. Images were acquired with a pixel size of 0.142 µm and a pinhole aperture of 1 Airy unit. Confocal images were analyzed on ImageJ (<https://imagej.nih.gov/ij/>). A median filter was applied and signal intensity adjusted on whole images for the counterstain Neurotrace wavelength, but fixed for the wavelength of secondary antibodies targeting *regucalcin1* (Fig. S8).

CRISPR/Cas9-mediated mutagenesis of *regucalcin1*. *Heliconius melpomene rosina* pupae were obtained from a commercial supplier (<https://www.butterflyfarm.co.cr>) and used to establish a stock in an external greenhouse at LMU Munich. We used *GeneiousPrime* v2021.1 to design 4 guide RNAs corresponding to N<sub>20</sub>NGG (on either strand), targeting exon1 and exon2 of *regucalcin1* (Table S2B), considering the gRNA efficiency scores predicted from (81), favoring GC-rich regions close to the PAM (NGG) sequence, and avoiding polymorphic sites in our butterfly stock. Introducing a deletion across exon1 and exon2 of *regucalcin1* permitted greater confidence that the KO would result in loss-of-function. This also allowed more rapid genotyping of individuals (i.e. requiring only a single PCR reaction vs. multiple steps required for Sanger-sequencing, see below). N<sub>20</sub>NGG sequences were screened for off-targets in the *H. melpomene* 2.5 genome with the BLAST function of Lepbase v4. Only guide RNAs that had unique seed regions 12bp upstream of the PAM were considered further to avoid off-targets.

Synthetic sgRNAs were ordered from *Synthego* (Redwood City, CA, US) and resuspended in TE (0.1mM EDTA, pH 8.0) buffer (Sigma Aldrich, St. Louis, MO, US). Cas9 protein (CP01, PNAbio) was reconstituted in nuclease-free water and 5% Phenol Red Solution (Sigma Aldrich), following the guidelines in (82). A mix of 4 gRNAs and later 2gRNAs and Cas9 protein (250:500ng/ $\mu$ l) was injected in eggs between 1 and 4.3 hours after laying, using a Femto Jet (Eppendorf, Hamburg, Germany).

To genotype mosaic generation zero (G0) individuals, we extracted gDNA from two caterpillar spikes at 4<sup>th</sup>/5<sup>th</sup> instar by squishing the spikes with a filter tip in 9  $\mu$ l NaOH solution (50mM), incubating at 95°C for 15 minutes, cooling the reaction on ice for 2 minutes and adding 1  $\mu$ l of Tris-HCl (1M) (Nicolas Gompel and Luca Livraghi pers. comm., modified from (83)). We then PCR-amplified a region of *regucalcin1* (Table S2), to screen for CRISPR/Cas9 mediated deletions as a result of non-homologous end-joining following multiple double-strand breaks predicted to result in a ~600bp DNA fragment (with deletion) instead of ~1900bp (no deletion).

We purified DNA from gel bands of the allele carrying the predicted deletion with a MinElute Gel Extraction Kit (QIAGEN) and ExoSap (Thermo Fisher) and Sanger-sequenced with a BigDye v1.1 kit (Thermo Fisher) with the Genomics Service Unit of LMU Munich to find that the same 2 gRNAs (Table S2) consistently mediated the introduction of a deletion and were therefore used for generating *regucalcin1* mKO butterflies in all experiments (survival/efficiency statistics for CRISPR experiments in Table S1). Although most CRISPR-mediated deletions were of the expected size (1300bp deletion), in a few mKO individuals the deletion varied in size (ranging from ~400bp to ~1500bp), probably due to variation in the DNA repair process. Nevertheless, we found that the boundaries of these deletions always coincided with either one of the two sgRNA target sites, likely generating similarly non-functional alleles. Individuals that were screened as mKO at the 4<sup>th</sup>/5<sup>th</sup> instar were subsequently confirmed as mKO by PCR on DNA extracted from adult brain, thorax or abdomen tissue with a DNAeasy Blood & Tissue kit. We extracted gDNA from at least two tissues among brain, thorax and abdomen from 40 individuals without deletion (ND), and sequenced their *regucalcin1* protein-coding region to screen for small frame-shift mutations/deletions following double-strand breaks at only one of the CRISPR target sites, which would not be detected by our PCR-fragment size screen. We found that only 1/40 individuals (2.5%) showed evidence of a CRISPR-mediated mutation at only one of the target sites not resulting in a large deletion. Thus, ND mKO individuals with small frame-shift mutations are rare and might have only marginally impacted the results (i.e., considered as ND instead of mKO). In contrast, mKO individuals had a substantial percentage of

cells carrying the deletion in their brain tissue (Fig. S9). This was repeated across multiple PCR reactions, and was further corroborated by Sanger-Sequencing, where we saw abrupt changes in the chromatogram at the level of the deletion (in whole-brain tissue gDNA mKO individuals) (Fig. S9D).

It is possible that the ~1300bp region between exon 1 and 2 targeted by our CRIPR/Cas9 experiments contains regulatory elements affecting the expression of other genes on chromosome 18. As such, we cannot absolutely discount the possibility that by introducing a deletion any phenotypic effects observed in mKO individuals are the result of having inadvertently disrupted the cis-regulatory region (CRE) of another gene besides from *regulcalcin1*. Nevertheless, we consider any phenotypic effects observed in mKO individuals much more likely to be the result of disrupting *regulcalcin1* function.

Drop test. To assay basic locomotor (flying) function of *regulcalcin1* mKO butterflies, we conducted a ‘drop test’ with mKO, ND or WT butterflies one day post-eclosion during the butterfly’s active hours (between 10:20 and 17:30). Each butterfly was held by the forewings 1.5 m above the ground at the center of a 2x2x2m cage and then released. This procedure was repeated 5 times for each butterfly, and individuals were considered to have ‘failed’ the test if they dropped directly on the ground (instead of flying) for all 5 trials. With the exception of three individuals (one mKO, one ND and one WT), all butterflies either dropped to the ground on all 5 trials, or flew on all five trials.

Optomotor assay. To determine whether *regulcalcin1* mKO butterflies show a visual (optomotor) response, i.e., an innate orienting response evoked by wide-field visual motion, we placed mKO, ND or WT butterflies >4 hours post-eclosion at the center of an experimental arena of 16 cm radius surrounded by a visual stimulus of alternating black and white stripes (84, 85). We used a visual stimulus with spatial frequency value (cycles-per-degree) of 0.2 cycles-per-degree (cpd). The width (in millimeters) of one cycle (a set of alternating black and white stripes) was calculated as  $cycle\ width = [(C/360) / a]$ , where ‘C’ is the circumference of the experimental arena (mm) and ‘a’ is the visual acuity (cpd). Butterflies were restrained in a clear PLEXIGLAS® cylinder and all assays were conducted at room temperature under illumination from an overhead LED lamp, and recorded with a GoPro camera (GoPro, San Mateo, CA, US) placed above the device. Butterflies were tested once they stopped crawling on the cylinder, which was followed by 6 rotations of the stimulus (alternating between clockwise and counterclockwise), each lasting 10 seconds, and running at a speed of three rotations per minute (3 rpm). A positive response was scored if the butterfly changed the orientation of its head/antenna in the direction of the moving stimulus and then re-oriented itself in the opposite direction when the direction of rotation was reversed, across the whole 1-minute trial (see Movie S1 for an example).

Courtship assay. mKO, ND and WT *H. melpomene* males were maintained together in a 2x2x2m cage in a greenhouse in Munich. As in our experiments in the tropics, butterflies were provided with *Lantana* and *Psiguria* flowers, as well as a sugar water supplement daily. All courtship trials were conducted between 11:00 and 17:00. We paired either an experimental mKO or ND >5days post explosion male with a WT male (matched for age, but otherwise chosen at random). This paired design allowed us to control for both the injection procedure, as well as prevailing conditions that might potentially influence male behavior. Individuals that failed the drop test

were excluded from courtship assays (as none survived five days post-eclosion). A WT virgin *H. melpomene* female (1-5 days post eclosion) was then introduced into the cage. As for our behavioral experiments in Colombia, 15-minute trials were divided into 1-minute intervals, and during each minute both the experimental and WT male were scored for three behaviors: flying, feeding, and courting (sustained hovering over or chasing the female for >3 seconds). The experimental cage was shaken every 5 minutes to stimulate butterfly activity. In the minute-interval following cage shaking, a flying occurrence was recorded only if it lasted for 10 uninterrupted seconds, or occurred after a butterfly had momentarily landed/stopped flying. The trials were stopped immediately if mating occurred (and the butterflies were gently separated). Trials were repeated up to 5 times for each experimental male (median=3). To further avoid biasing our results, we excluded from trials a single mKO male that did not fly, court or feed during all 4 trials in which it was tested (though this more conservative approach does not qualitatively affect our results).

As with data from our behavioral trials in Colombia, we tested for differences in relative courtship activity between mKO and ND males using generalized linear mixed models (GLMMs) with binomial error structure and logit link function (implemented with the R package lme4). This time the proportion of minutes courting females by experimental (i.e., mKO or ND) vs WT males was the dependent variable and the experimental male type (mKO or ND) was set as a fixed explanatory factor. We tested significance by comparing this model to a null model, excluding experimental type as an explanatory variable, with a likelihood ratio test. Once again, experimental male ID was included as an individual level random factor in all models to account for overdispersion. To determine whether mKO and ND males differ in more general motor activities, we repeated these analyses, but this time with the proportion of minutes spent flying or feeding by experimental versus WT males. Estimated marginal means and confidence intervals were extracted using *emmeans*.

Patternize analysis. To determine whether *regucalcin1* mKO affects wing color patterns in *H. melpomene rosina*, we quantified and compared color patterns of mKO and ND butterflies using *patternize* (86). Wing pictures were taken in RAW format with a Fujifilm X-T3 camera with a Fujifilm 35mm F1.4 R lens, using a white-diffusion sheet (Lee filters 252) to homogenize lighting from two overhead LED lamps. The white balance of each image was then adjusted with the *Curves* feature (constant settings) in Adobe Photoshop CC 2019 (Adobe, CA, USA), to mask either one of the butterfly forewings (marked with a marker pen to keep track of individual butterflies ID) and to remove the background. To align wing images, we positioned 18 and 16 landmarks respectively (as suggested in the *patternize* package) at vein intersections on the forewings and hindwings for each sample (Fig. S10A). A *thin plate spline* transformation was then used to align landmarks to a common (arbitrarily chosen) reference sample for each of 4 groups (mKO males, mKO females, ND males, ND females) and each 4 patterns (forewing dorsal, forewing ventral, hindwing dorsal, hindwing ventral) independently. To compare pattern size and shape among samples, the red, green, and blue (RGB) values were extracted for each pattern of each group separately using *patternize*, with color threshold “colOffset”, and the relative size of the pattern was calculated as the proportion of the pattern area over the total wing area (of the same wing) using the *patArea* function in *patternize*. Differences in color pattern among groups were calculated by subtracting the pattern frequencies with the “sumRaster” function in *patternize*. The resulting rasters were analyzed using Gower’s dissimilarity measure (87) in the R package *StatMatch*, as commonly used for *patternize* data (for example in reef

fishes, (88)), to determine statistically significant differences in pattern spatial distribution among groups (Fig. S10).

## Supplementary figures and tables

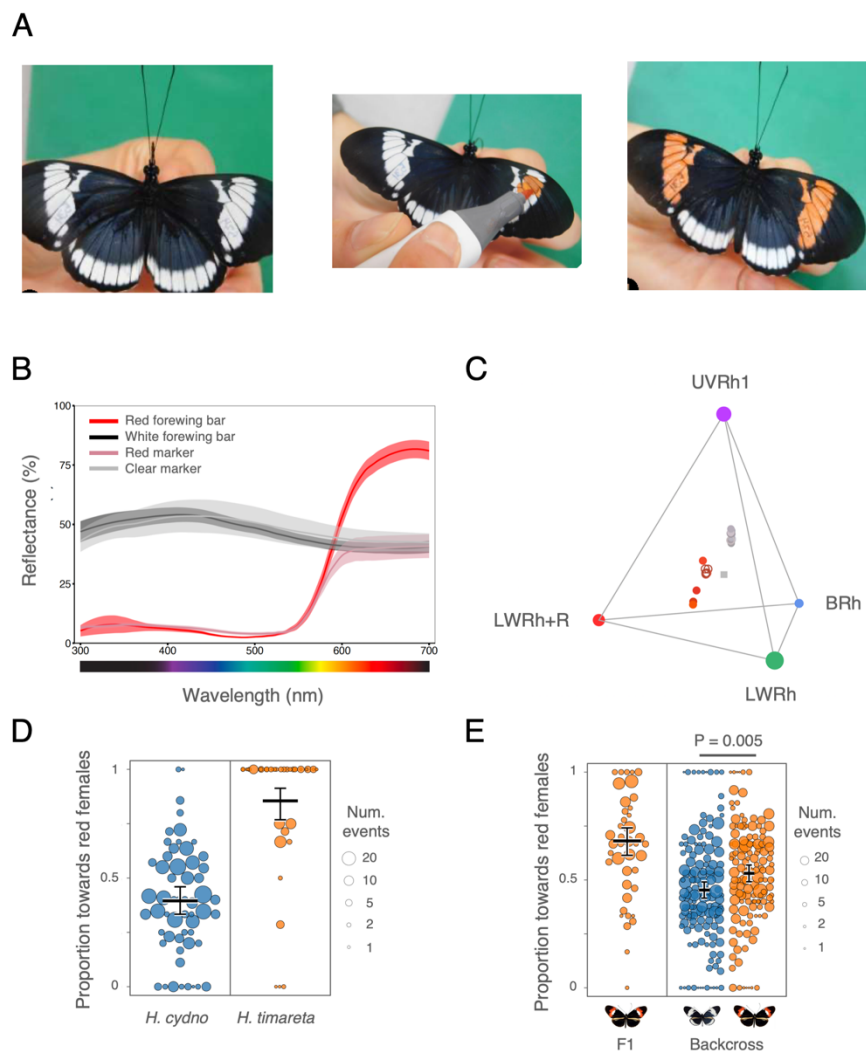


**Fig. S1. Species mating preferences and the behavioral QTL on chromosome 18 are visually guided.** (A) Manipulation of *H. cydno* female forewing color with a red marker pen (photo credit: Tal Kleinhause Gedalyahou). (B) Reflectance spectra of the natural red and red-painted forewing bars, as well as of the white and clear-painted (transparent marker) forewing bars averaged across 4 *Heliconius timareta tristero*, 4 painted *H. cydno cydno*, 9 *H. c. cydno* and 4 painted *H. c. cydno* samples respectively. Shaded regions represent  $\pm 1$  standard error. (C) Tetrahedral color space, *i.e.*, predicted stimulation of different photoreceptor cell types, for the different forewing reflectances, using a tetrachromatic model with *H. melpomene* photoreceptor cell sensitivities (49). Corners indicate photoreceptor cell-type maximum sensitivities: UV-Rhodopsin1 (360 nm), blue-Rhodopsin (470nm), long wavelength-Rhodopsin without (570nm) and with red filtering pigments (+R) (590nm). Solid circles indicate unmanipulated forewings ( $n=5$ ), open circles indicate painted forewings ( $n=5$ ), and the solid square indicates the achromatic point of equal stimulation for all photoreceptors. (D) Proportion of courtship time directed towards red painted *H. c. cydno* females relative to white (transparently painted) *H. cydno* females, by *H. timareta* and *H. cydno* males, and (E) by F1 hybrids and backcross to *H. cydno* hybrid males. Orange points represent individuals

that are heterozygous (i.e., *H. cyd/H. tim.*) and blue points represent individuals that are homozygous for (i.e., *H. cyd./H. cyd.*) *H. cydno* alleles at the *optix* locus on chromosome 18 (and tightly linked regions, including the QTL peak). Dot size is scaled to the number of total minutes a male responded to either female type. Estimated marginal means and their 95% confidence intervals are displayed with black bars.

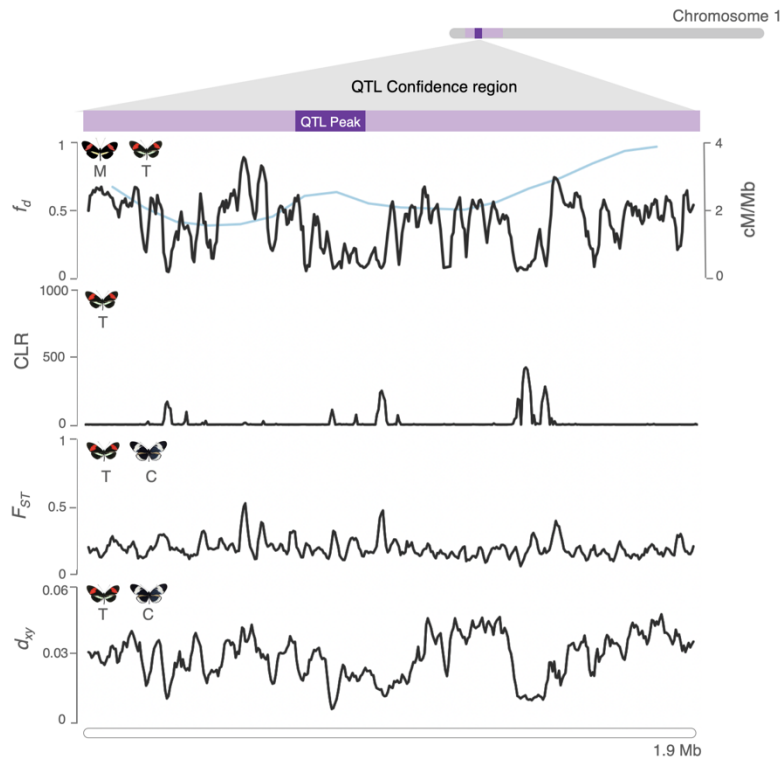


**Fig. S2. Genomic signatures of adaptive introgression and divergence at the behavioral QTL on chromosome 1.** Top panel: Admixture proportion values between *H. melpomene* and *H. timareta* at the behavioral QTL region on chromosome 1. Recombination rates (as estimated in (31)) overlaid in blue. Second panel: composite likelihood ratio (CLR) of a selective sweep in *H. timareta*. Third and fourth panels display fixation index ( $F_{ST}$ ) and  $d_{xy}$ , between *H. timareta* and *H. cydno*.

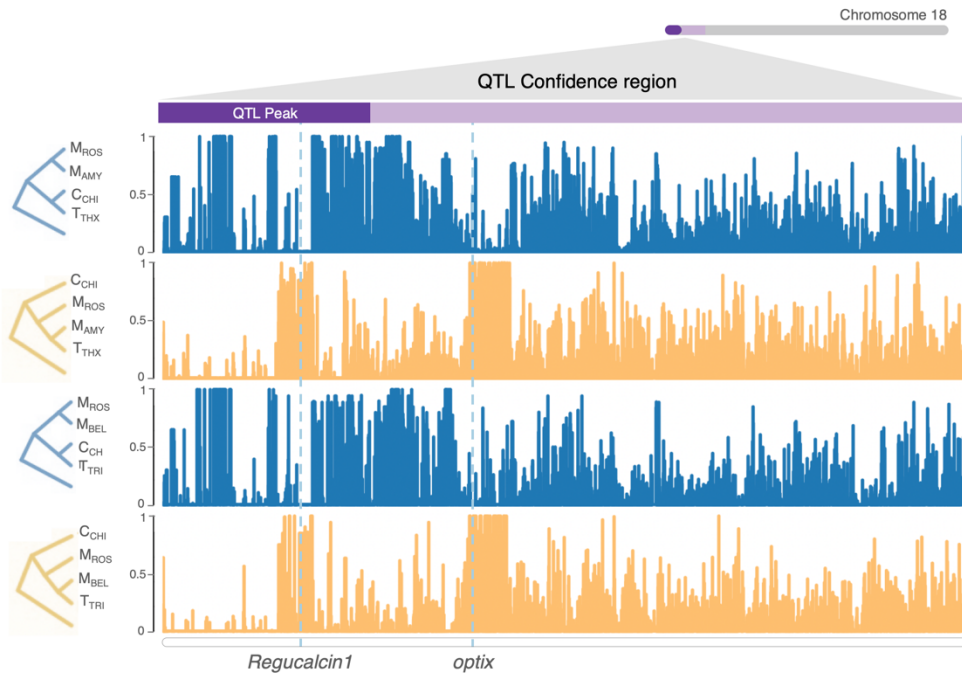


**Fig. S3. Sharing of alleles between different populations of red-preferring species at *regucalcin1* and *optix*.** Topology weightings, i.e., proportion of a particular phylogenetic tree over all possible rooted trees, along the behavioral QTL region on chromosome 18 ( $x$ -axis represent physical position). The “species” tree (expected species relationships: *H. timareta* more closely related to *H. cydno* than *H. melpomene*) is represented in blue, the “introgression” tree (where *H. timareta* clusters with its sympatric *H. melpomene* co-mimic) in orange. Top two panels: focal populations of *H. timareta* and *H. melpomene* from Peru ( $M_{AMY} = H. m. amaryllis$  and  $T_{THX} = H. t. thelxinoe$ ); other *H. melpomene* and *H. cydno* population are from Panama ( $M_{ROS} = H. m. rosina$  and  $C_{CHI} = H. cydno\ chionius$ ). Bottom panels: focal populations from Colombia ( $M_{BEL} = H. m. bellula$  and  $T_{TRI} = H. t. tristero$ ). *H. numata* was used as outgroup. Gene coordinates of *regucalcin1* (candidate behavioral gene) and *optix* (color pattern gene) are highlighted by vertical light blue dotted lines.

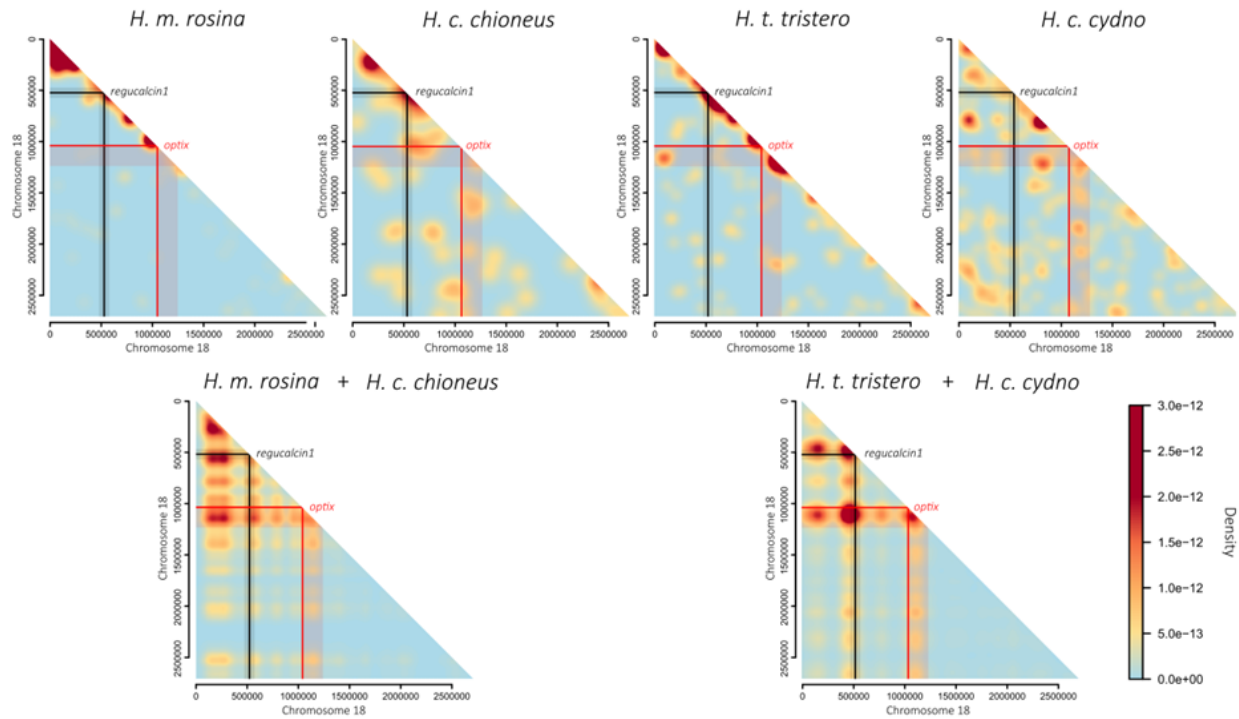


**Fig. S4. Density maps of Linkage Disequilibrium (LD) at the behavioral QTL on chromosome 18.** The top row shows LD patterns within populations, whereas the bottom row shows LD calculated over pairs of populations, with different color pattern and corresponding preferences. Intense red colors indicate a high density of SNP pairs with  $R^2$  values larger than 0.8. Black and red lines indicate the position of the *regucalcin1* and *optix* gene, respectively. Similarly, gray shaded areas include putative CRE candidates for *regucalcin1* and the red shaded area includes the genomic region associated with *optix* expression and evolution, as identified from chromatin and selective sweep studies (see supplementary methods above).

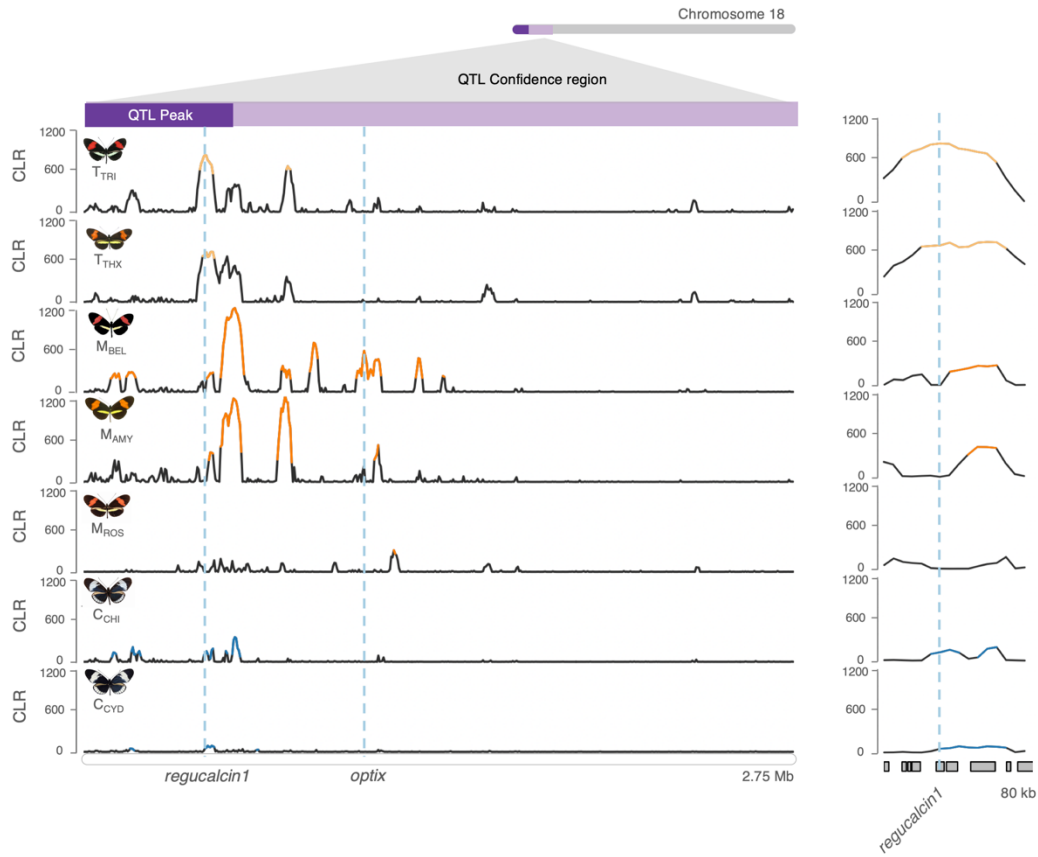


**Fig. S5. Evidence for a selective sweep at the *regucalcin1* locus across different *Heliconius* populations.** Composite likelihood ratio (CLR) of a selective sweep in different *Heliconius* populations across the QTL region on chromosome 18. Top 1% quantile values are highlighted with colors. Note that i) the highest support for a selective sweep in *H. melpomene* populations is centered at ~100 kb from the *regucalcin1* locus and likely represent a more recent selective sweep at a locus other than *regucalcin1* ii) the considerably lower absolute CLR score in *H. cydno* populations compared to *H. timareta* populations at *regucalcin1* could represent the effect of background selection (removal of deleterious variants), remnants of an old selective sweep or noise instead of positive selection. M<sub>AMY</sub> = *H. melpomene amaryllis* (Peru), M<sub>BEL</sub> = *H. melpomene bellula* (Colombia), M<sub>ROS</sub> = *H. melpomene rosina* (Panama), M<sub>MEL</sub> = *H. melpomene melpomene* (Colombia), T<sub>TRI</sub> = *H. timareta tristero* (Colombia), T<sub>THX</sub> = *H. timareta thelxinoe* (Peru), C<sub>CHI</sub> = *H. cydno chioneus* (Panama), C<sub>CYD</sub> = *H. cydno cydno* (Colombia).

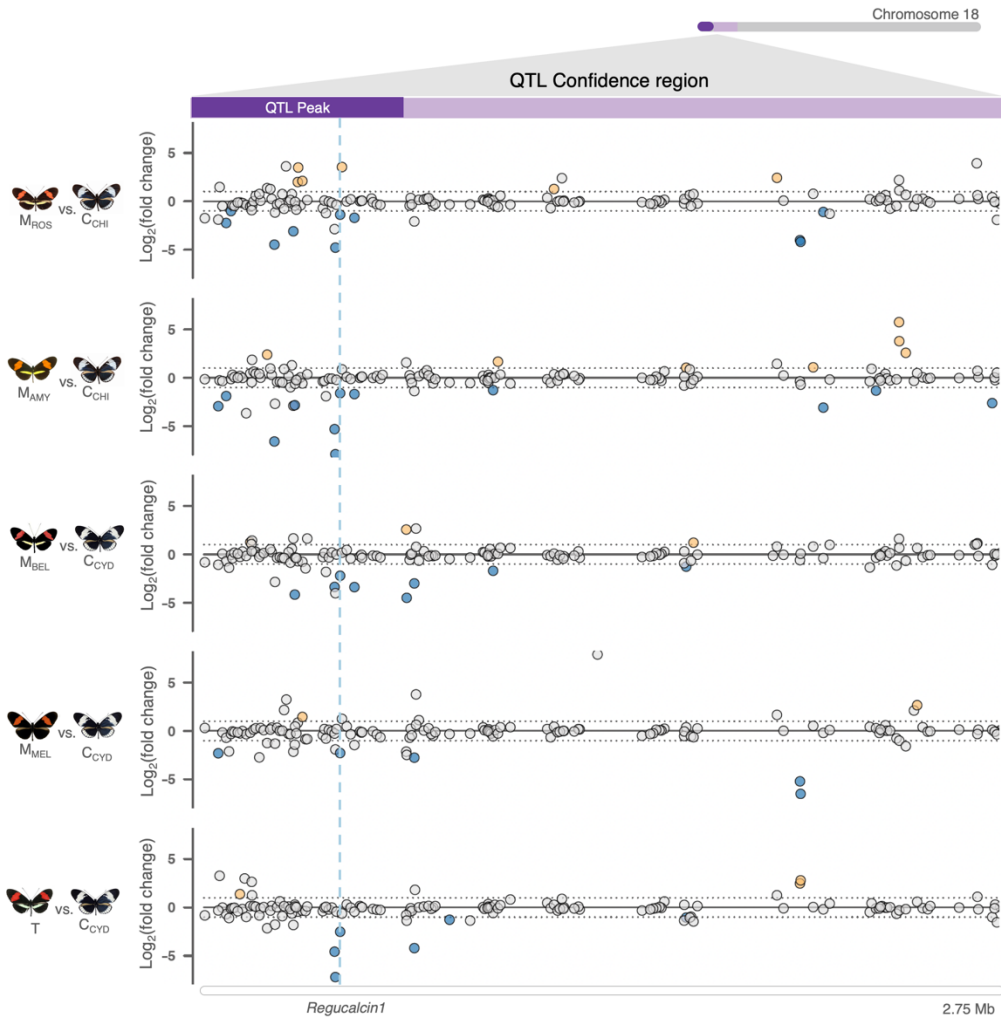


**Fig. S6. Differential expression across populations at the preference QTL region on chromosome 18.** Points correspond to individual genes and the y-axis indicates the  $\log_2$  (fold-change) for each “red-preferring” vs “white preferring” subspecies comparison. The QTL peak, and the rest of the QTL confidence interval on chromosome 18 are shown on top in dark and light purple respectively (x-axis represents physical position). The two horizontal dashed lines (at y-values of 1 and -1) indicate a 2-fold change in expression. Genes showing a significant 2-fold+ change in expression level between groups are highlighted in orange and blue, where orange indicate a 2-fold higher expression level in *H. melpomene* subspecies or *H. timareta*, whereas blue a 2-fold higher expression level in *H. cydno*. A vertical dashed blue line highlights the only gene that is differentially expressed between all comparisons: *regucalcin1* (higher expression level in *H. cydno* populations). M<sub>AMY</sub> = *H. melpomene amaryllis* (raised in Panama), M<sub>BEL</sub> = *H. melpomene bellula* (raised in Colombia), M<sub>ROS</sub> = *H. melpomene rosina* (raised in Panama), M<sub>MEL</sub> = *H. melpomene melpomene* (raised in Colombia), T<sub>TRI</sub> = *H. timareta tristero* (raised in Colombia), C<sub>CHI</sub> = *H. cydno chioneus* (raised in Panama), C<sub>CYD</sub> = *H. cydno cydno* (raised in Colombia).

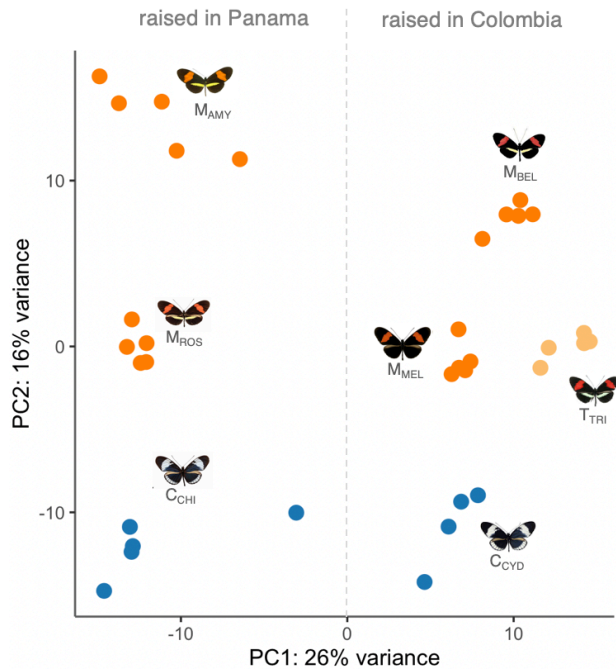


**Fig. S7. Brain and eye transcriptomic profiles cluster by rearing environment and species.** Principal component analysis (PCA) of gene expression levels for the 500 genes with most variable expression level across brain tissue samples from different species. Samples are color-coded by species. A vertical dotted line has been drawn to indicate the division (PC1) between individuals that were raised in Panama (*H. c. chioneus* (C<sub>CHI</sub>) and *H. m. rosina* (M<sub>ROS</sub>) as previously described (27)) and in Colombia. Interestingly, *H. timareta* clusters more closely to *H. melpomene* (by visual preference phenotype) than to *H. cydno* (by phylogeny), suggesting broad convergence in neuro-transcriptomic profiles between sympatric, hybridizing populations of *H. melpomene* and *H. timareta*, raised in common garden conditions. M<sub>AMY</sub> = *H. melpomene amaryllis* (raised in Panama), M<sub>BEL</sub> = *H. melpomene bellula* (raised in Colombia), M<sub>ROS</sub> = *H. melpomene rosina* (raised in Panama), M<sub>MEL</sub> = *H. melpomene melpomene* (raised in Colombia), T<sub>TRI</sub> = *H. timareta tristero* (raised in Colombia), C<sub>CHI</sub> = *H. cydno chioneus* (raised in Panama), C<sub>CYD</sub> = *H. cydno cydno* (raised in Colombia).

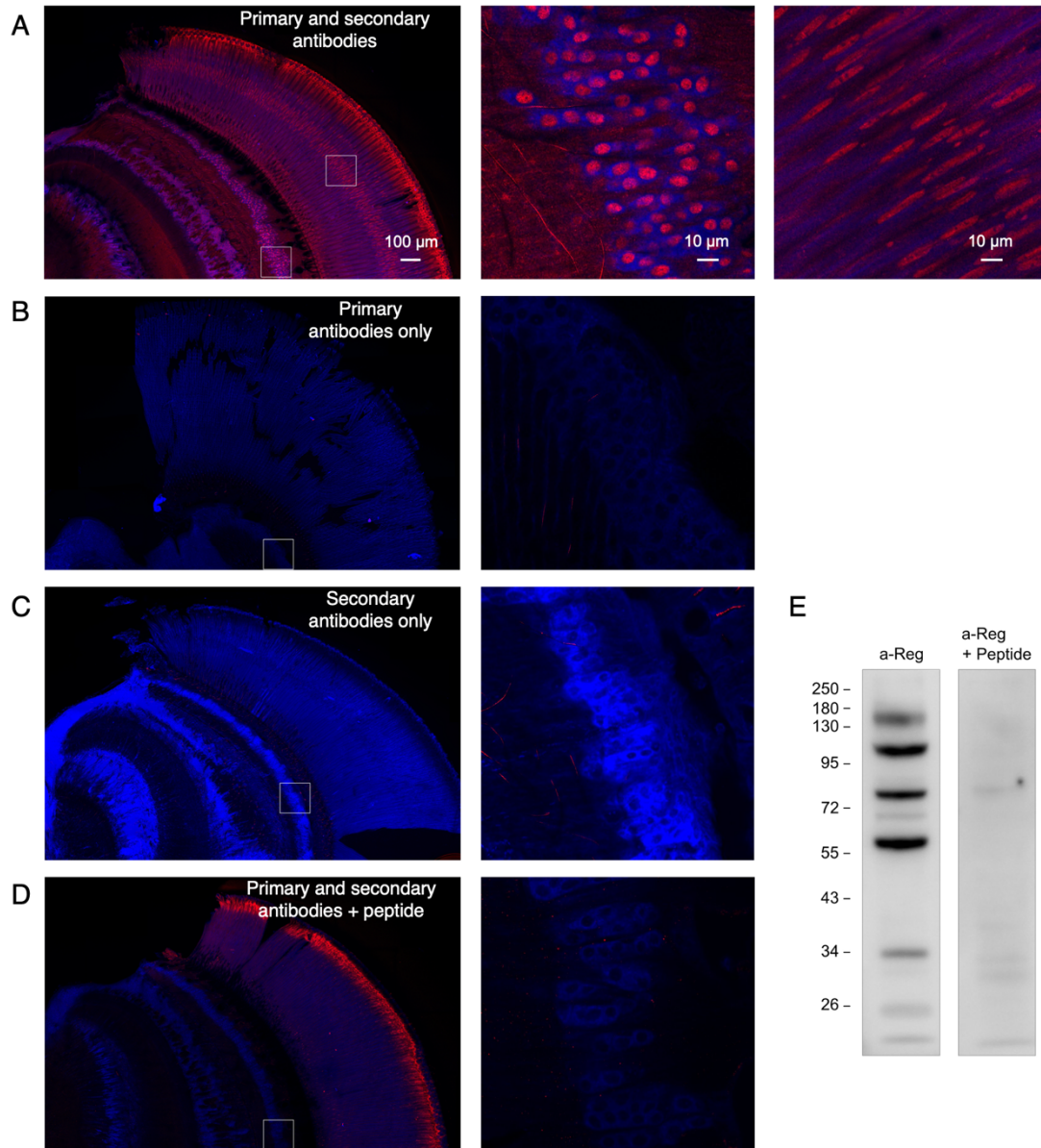


**Fig. S8. Controls for antibody specificity.** The left column shows immunostainings (red) of slices containing brain and eye brain tissue (maximum intensity Z-projections) counterstained by neurotrace fluorescent Nissl stain (blue), and the middle column shows a zoom in the lamina region of the optic lobe (single confocal plane). (A) Standard immunostaining with *regucalcin1* antibodies (incubation with both primary and secondary antibodies) showing broad patterns of regucalcin1 expression across the brain and eye; the right panel shows a zoom in the eye tissue/photoreceptor cells. We additionally performed three negative controls to test *regucalcin1* antibodies staining specificity: (B) Tissue incubated with primary antibodies but no secondary antibodies; (C) Tissue incubated with secondary antibodies but no primary antibodies; and (D) tissue incubated with primary and secondary antibodies, where the solution containing primary antibodies also contained the blocking peptide and had previously been incubated with the blocking peptide for 2 hours. Staining within somas and neuropil is absent in the three

negative controls. We note that non-specific staining is observed in the outer pigmented layer of the eye, as indicated by staining in this region when tissue was incubated with both antibodies and excess peptide (**D**). (**E**) Western blot confirming the presence of a ~34 kDa band (gel on the left) that corresponds to the predicted size of the *regucalcin1* protein (33.8 kDa). This band disappears (gel on the right) in the presence of blocking peptide (due to antibodies binding to the excess peptide). Additional immunoreactive bands as in (89) also disappear in the presence of the blocking peptide.

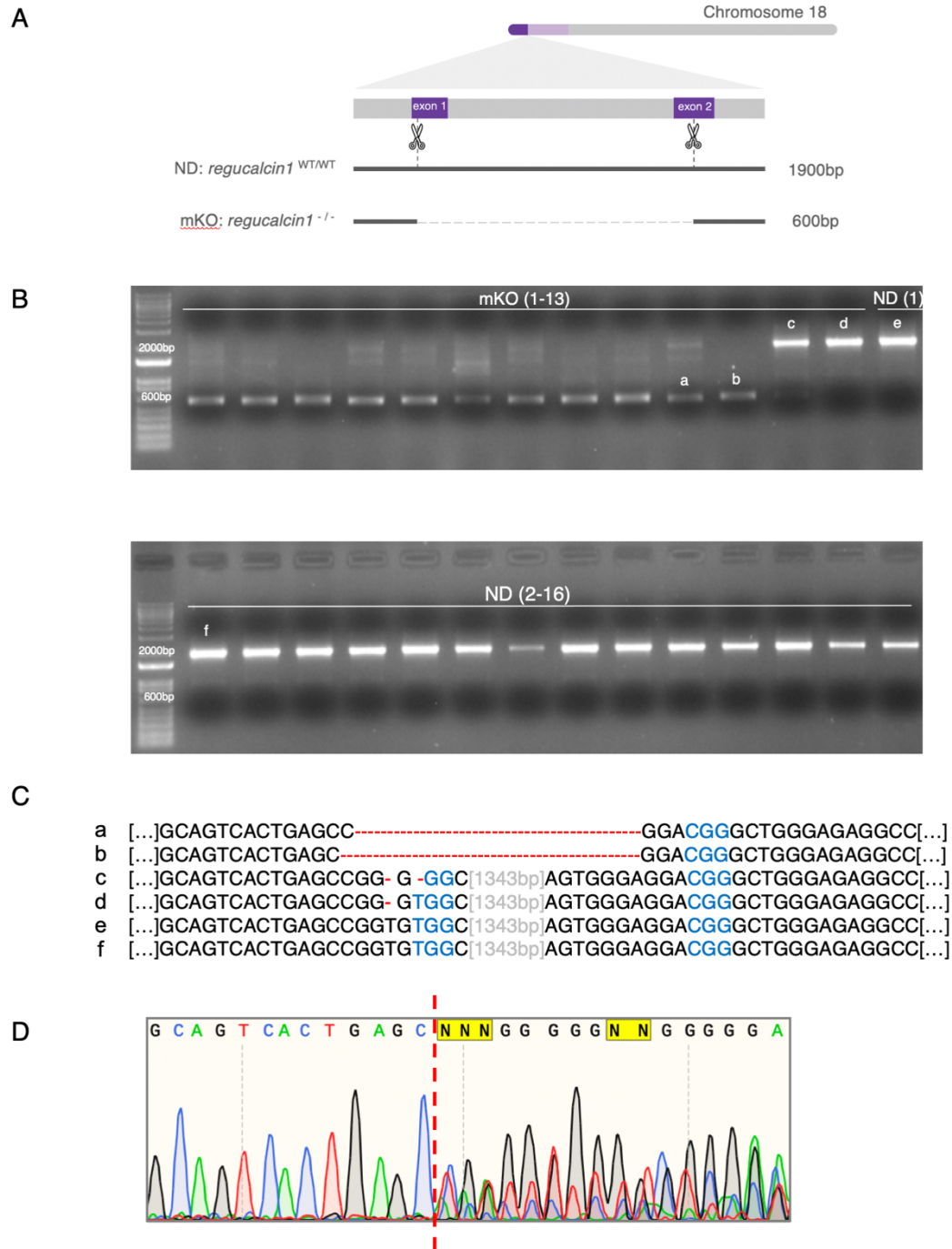


**Fig. S9. A high percentage of cells show *regucalcin1* knock-out in G0 mosaic individuals. (A)** Schematic representation of the *regucalcin1* locus with the target sites of the small guide RNAs and resulting CRISPR/Cas9-mediated deletion. **(B)** Gel electrophoresis of PCR products of the *regucalcin1* locus from DNA extracted from whole brain tissue of mKO and ND males that were tested in courtship assays (note that 1 ND male sample was not included for space constraints on the gel, and that DNA extraction could not be carried out for 3 ND individuals, whose bodies could not be recovered). We note that while PCR amplification suggests that a substantial number of

cells in brain tissue carry a deletion at the regucalcin1 locus for the first eleven individuals shown in the gel (i.e., with brighter bands at ~600bp than at 1900bp), this should be considered an approximation of the level of mosaicism. There may not be a simple relationship between the PCR results and the percentage of cells expressing non-functional copies of regucalcin1 protein. Nevertheless, the marked difference in bands' brightness is consistent across multiple samples and was repeatable across independent PCR amplifications. **(C)** Examples of nucleotide sequences for alleles carrying and not carrying the deletion (as inferred with Sanger-sequencing of DNA purified from the respective gel bands). Note that for sample mKO 12 (c) there is also a small percentage of cells with deletion, whereas for sample mKO 13 (d) only a single-nucleotide frame-shift mutation. **(D)** mKO individuals were further corroborated by Sanger-Sequencing, where we saw abrupt changes in the chromatogram at the level of the deletion. This is shown in the example chromatogram for a mKO assigned individual, where we were unable to recover the 'correct' not-deleted sequence, i.e., to the right of the vertical dashed red line.

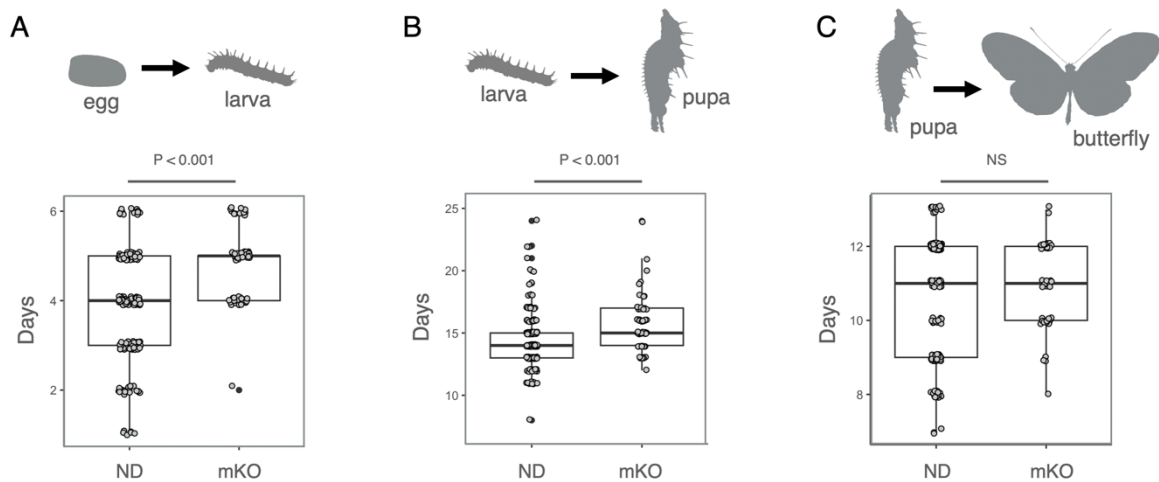


**Fig. S10. CRISPR/Cas9 mediated knock-out of *regucalcin1* delays development in its early stages.** Days it took to develop (A) from egg to larva (unpaired *t*-test:  $P < 0.001$ ) (B) from larva to pupa (unpaired *t*-test:  $P < 0.001$ ) and (C) from pupa to imago (adult) (unpaired *t*-test:  $P > 0.05$ ) for individuals without (ND) and with deletion (mKO) at the *regucalcin1* locus.

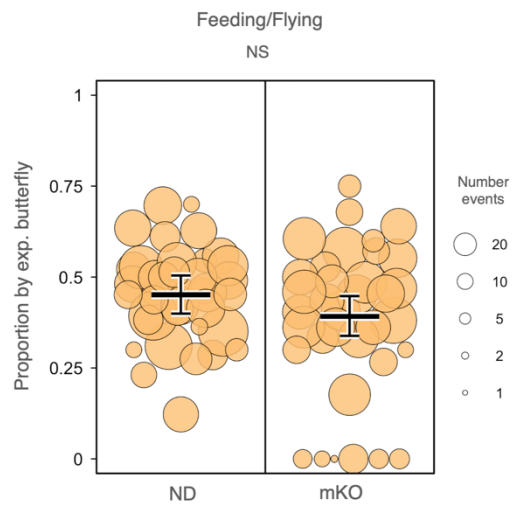


**Fig. S11. No significant change in flying and feeding behaviors caused by *regucalcin1* knock-out.** Proportion of time spent flying and/or feeding by ND individuals (left) and *regucalcin1* mKO individuals (right) relative to wild-type butterflies (female and male individual tested, females were tested as of 1-day of age). These include four females that did not pass the drop test and (two additional males that) did not show any flying or feeding activity (values = 0). Dot size is scaled to the number of total minutes individuals flew and/or fed during the experiments.

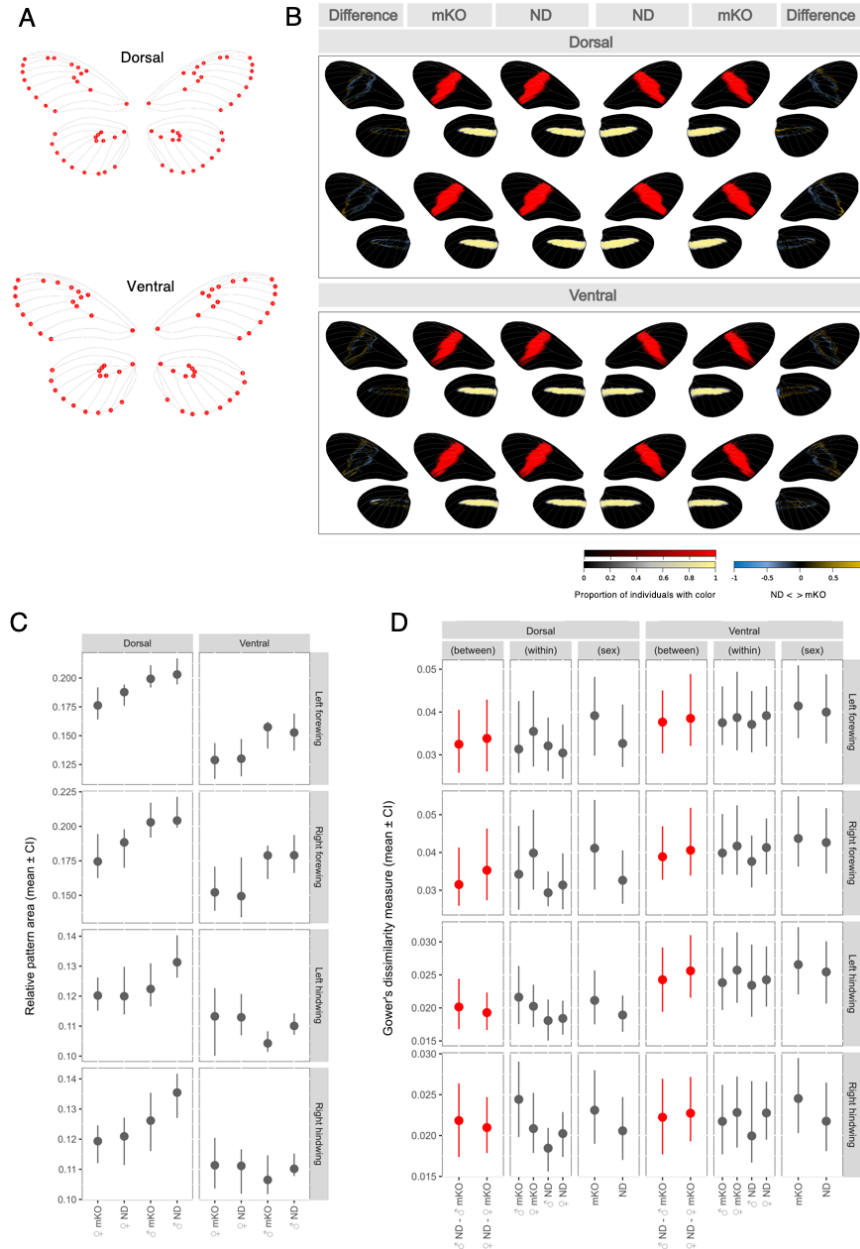


**Fig. S12. No evidence for an effect on color pattern in *regucalcin1* mKO individuals.** (A) Landmarks placed at the intersection of the forewing and hindwing veins for dorsal and ventral wing sides. (B) Average color patterns (central columns) and differences in color pattern (leftmost and rightmost columns) between *H. melpomene rosina* mKO and ND (i.e., with and without deletion at *regucalcin1*) individuals, analyzed separately by sex, forewing (FB) and hindwing band (HB), and dorsal and ventral sides (sample sizes: 26 mKO females, 20 mKO males, 23 ND females and 19 ND males). Yellow indicates higher presence of FB/HB in mKO butterflies and blue indicates higher presence of FB/HB in ND butterflies. (C) Average pattern area of FB and HB for each group, with 95% confidence intervals. (D) Mean Gower's dissimilarity measure of FB and HB between-group, within-group and between sex of the same group, with 95% confidence intervals. No significant difference detected.

# eggs injected	within time (h)	# larvae hatched	% hatched	# DNA extraction worked	# PCR worked	#deletion	% deletion
81	2.7 - 3.7	7	9%	3	3	2	67%
147	2.0 - 3.4	33	22%	22	15	3	20%
163	3.6 - 4.3	22	13%	7	7	0	0%
NA	NA	NA	NA	7	4	1	25%
107	3.5	24	22%	13	11	0	0%
70	3	17	24%	14	9	2	22%
76	3.6	16	21%	15	15	3	20%
61	1 - 3.5	7	11%	5	5	4	80%
71	2.5 - 3.5	14	20%	12	8	6	75%
57	3	15	26%	13	10	2	20%
52	2-3	15	29%	12	11	0	0%
121	2.7 - 3.6	46	38%	41	32	11	34%
103	2.6	37	36%	33	33	12	36%
107	3.9	26	24%	22	18	1	5%
99	2.6	14	14%	12	12	4	33%
49	3.3	7	14%	7	7	0	0%
73	4.2	28	38%	26	26	10	38%
70	3	32	46%	15	15	0	0%
63	2.8	21	33%	15	13	1	8%
Tot. 254						Tot. 62	Tot. 24%

**Table S1. Survival and efficiency statistics in CRISPR/Cas9 experiments.** In all the injections above the same concentration and mix of 2 sgRNAs targeting *regucalcin1* were used (see Table S2), with a sgRNA to Cas9 concentration of 250/500 ng/ $\mu$ l.

**A**

Chromosome	Orientation	Sequence (5' to 3')
1	forward	CGCGCCATAATTTAGACATC
1	reverse	TGATAGTCCATACCTGCAAC
1	forward	TCATTGATTTTGACCCGACT
1	reverse	CATACTCGGCCGTGTTATAC
18	forward	GACATGCCAGGCTTCATAAT
18	reverse	TGAATTACCTGAGAGCCATC

**B**

Strand/location	Target sequence (5' to 3', PAM not included)
+/exon1	AAGCAGTCACTGAGCCGGTG
+/exon2	GTAGTGGTCGTACAGTGGGA

**C**

Purpose	Orientation	Sequence (5' to 3')
amplify	forward	GCTCATGTCCGTTTGTCTAT
amplify	reverse	ATCGATATCCACCTCCATCA
sequence – exon1	forward	TTAAATGTGACAGCCGAGTT
sequence – exon2	reverse	TACCAACAAACAATCTGCCT

**Table S2. Primer and guide RNA sequences.** (A) PCR primer sequences for obtaining genotype information at QTL locations (B) sgRNA sequences for CRISPR knock-outs of *regucalcin1* (C) PCR primer sequences for detecting *regucalcin1* KO occurrence.

## References and Notes

1. I. C. Cuthill, W. L. Allen, K. Arbuckle, B. Caspers, G. Chaplin, M. E. Hauber, G. E. Hill, N. G. Jablonski, C. D. Jiggins, A. Kelber, J. Mappes, J. Marshall, R. Merrill, D. Osorio, R. Prum, N. W. Roberts, A. Roulin, H. M. Rowland, T. N. Sherratt, J. Skelhorn, M. P. Speed, M. Stevens, M. C. Stoddard, D. Stuart-Fox, L. Talas, E. Tibbetts, T. Caro, The biology of color. *Science* **357**, eaan0221 (2017).
2. A. Orteu, C. D. Jiggins, The genomics of coloration provides insights into adaptive evolution. *Nat. Rev. Genet.* **21**, 461–475 (2020).
3. U. Knief, C. M. Bossu, N. Saino, B. Hansson, J. Poelstra, N. Vijay, M. Weissensteiner, J. B. W. Wolf, Epistatic mutations under divergent selection govern phenotypic variation in the crow hybrid zone. *Nat. Ecol. Evol.* **3**, 570–576 (2019).
4. S. Ansai, K. Mochida, S. Fujimoto, D. F. Mokodongan, B. K. A. Sumarto, K. W. A. Masengi, R. K. Hadiaty, A. J. Nagano, A. Toyoda, K. Naruse, K. Yamahira, J. Kitano, Genome editing reveals fitness effects of a gene for sexual dichromatism in Sulawesian fishes. *Nat. Commun.* **12**, 1350 (2021).
5. S. M. Van Belleghem, A. A. Ruggieri, C. Concha, L. Livraghi, L. Hebberecht, E. S. Rivera, J. G. Ogilvie, J. J. Hanly, I. A. Warren, S. Planas, Y. Ortiz-Ruiz, R. Reed, J. J. Lewis, C. D. Jiggins, B. A. Counterman, W. O. McMillan, R. Papa, High level of novelty under the hood of convergent evolution. *Science* **379**, 1043–1049 (2023).
6. M. Liang, W. Chen, A. M. LaFountain, Y. Liu, F. Peng, R. Xia, H. D. Bradshaw, Y.-W. Yuan, Taxon-specific, phased siRNAs underlie a speciation locus in monkeyflowers. *Science* **379**, 576–582 (2023).
7. V. Ficarrota, J. J. Hanly, L. S. Loh, C. M. Francescutti, A. Ren, K. Tunström, C. W. Wheat, A. H. Porter, B. A. Counterman, A. Martin, A genetic switch for male UV iridescence in an incipient species pair of sulphur butterflies. *Proc. Natl. Acad. Sci. U.S.A.* **119**, e2109255118 (2022).
8. M. Unbehend, G. M. Kozak, F. Koutroumpa, B. S. Coates, T. Dekker, A. T. Groot, D. G. Heckel, E. B. Dopman, bric à brac controls sex pheromone choice by male European corn borer moths. *Nat. Commun.* **12**, 2818 (2021).
9. P. Brand, I. A. Hinojosa-Díaz, R. Ayala, M. Daigle, C. L. Yurrita Obiols, T. Eltz, S. R. Ramírez, The evolution of sexual signaling is linked to odorant receptor tuning in perfume-collecting orchid bees. *Nat. Commun.* **11**, 244 (2020).
10. O. M. Ahmed, A. Avila-Herrera, K. M. Tun, P. H. Serpa, J. Peng, S. Parthasarathy, J.-M. Knapp, D. L. Stern, G. W. Davis, K. S. Pollard, N. M. Shah, Evolution of mechanisms that control mating in *Drosophila* males. *Cell Rep.* **27**, 2527–2536.e4 (2019).
11. R. M. Merrill, P. Rastas, S. H. Martin, M. C. Melo, S. Barker, J. Davey, W. O. McMillan, C. D. Jiggins, Genetic dissection of assortative mating behavior. *PLoS Biol.* **17**, e2005902–e2005921 (2019).

12. M. R. Kronforst, L. G. Young, D. D. Kapan, C. McNeely, R. J. O'Neill, L. E. Gilbert, Linkage of butterfly mate preference and wing color preference cue at the genomic location of *wingless*. *Proc. Natl. Acad. Sci. U.S.A.* **103**, 6575–6580 (2006).
13. S. R. Pryke, Sex chromosome linkage of mate preference and color signal maintains assortative mating between interbreeding finch morphs. *Evolution* **64**, 1301–1310 (2010).
14. N. L. Chamberlain, R. I. Hill, D. D. Kapan, L. E. Gilbert, M. R. Kronforst, Polymorphic butterfly reveals the missing link in ecological speciation. *Science* **326**, 847–850 (2009).
15. O. Seehausen, Y. Terai, I. S. Magalhaes, K. L. Carleton, H. D. J. Mrosso, R. Miyagi, I. van der Sluijs, M. V. Schneider, M. E. Maan, H. Tachida, H. Imai, N. Okada, Speciation through sensory drive in cichlid fish. *Nature* **455**, 620–626 (2008).
16. J. Crane, Imaginal behaviour of a Trinidad butterfly, *Heliconius erato hydara* Hewitson, with special reference to the social use of color. *Zoologica* **40**, 167–196 (1955).
17. K. Darragh, S. Vanjari, F. Mann, M. F. Gonzalez-Rojas, C. R. Morrison, C. Salazar, C. Pardo-Diaz, R. M. Merrill, W. O. McMillan, S. Schulz, C. D. Jiggins, Male sex pheromone components in *Heliconius* butterflies released by the androconia affect female choice. *PeerJ* **5**, e3953 (2017).
18. C. D. Jiggins, R. E. Naisbit, R. L. Coe, J. Mallet, Reproductive isolation caused by colour pattern mimicry. *Nature* **411**, 302–305 (2001).
19. R. D. Reed, R. Papa, A. Martin, H. M. Hines, B. A. Counterman, C. Pardo-Diaz, C. D. Jiggins, N. L. Chamberlain, M. R. Kronforst, R. Chen, G. Halder, H. F. Nijhout, W. O. McMillan, optix drives the repeated convergent evolution of butterfly wing pattern mimicry. *Science* **333**, 1137–1141 (2011).
20. N. J. Nadeau, C. Pardo-Diaz, A. Whibley, M. A. Supple, S. V. Saenko, R. W. R. Wallbank, G. C. Wu, L. Maroja, L. Ferguson, J. J. Hanly, H. Hines, C. Salazar, R. M. Merrill, A. J. Dowling, R. H. ffrench-Constant, V. Llaurens, M. Joron, W. O. McMillan, C. D. Jiggins, The gene cortex controls mimicry and crypsis in butterflies and moths. *Nature* **534**, 106–110 (2016).
21. A. Martin, R. Papa, N. J. Nadeau, R. I. Hill, B. A. Counterman, G. Halder, C. D. Jiggins, M. R. Kronforst, A. D. Long, W. O. McMillan, R. D. Reed, Diversification of complex butterfly wing patterns by repeated regulatory evolution of a Wnt ligand. *Proc. Natl. Acad. Sci. U.S.A.* **109**, 12632–12637 (2012).
22. E. L. Westerman, N. W. VanKuren, D. Massardo, A. Tenger-Trolander, W. Zhang, R. I. Hill, M. Perry, E. Bayala, K. Barr, N. Chamberlain, T. E. Douglas, N. Buerkle, S. E. Palmer, M. R. Kronforst, Aristaless controls butterfly wing color variation used in mimicry and mate choice. *Curr. Biol.* **28**, 3469–3474.e4 (2018).
23. N. B. Edelman, P. B. Frandsen, M. Miyagi, B. Clavijo, J. Davey, R. B. Dikow, G. García-Accinelli, S. M. Van Belleghem, N. Patterson, D. E. Neafsey, R. Challis, S. Kumar, G. R. P. Moreira, C. Salazar, M. Chouteau, B. A. Counterman, R. Papa, M. Blaxter, R. D. Reed, K. K. Dasmahapatra, M. Kronforst, M. Joron, C. D. Jiggins, W. O. McMillan, F. Di Palma, A. J. Blumberg, J. Wakeley, D. Jaffe, J. Mallet, Genomic architecture and introgression shape a butterfly radiation. *Science* **366**, 594–599 (2019).

24. R. W. R. Wallbank, S. W. Baxter, C. Pardo-Diaz, J. J. Hanly, S. H. Martin, J. Mallet, K. K. Dasmahapatra, C. Salazar, M. Joron, N. Nadeau, W. O. McMillan, C. D. Jiggins, Evolutionary novelty in a butterfly wing pattern through enhancer shuffling. *PLOS Biol.* **14**, e1002353 (2016).
25. Heliconius Genome Consortium, Butterfly genome reveals promiscuous exchange of mimicry adaptations among species. *Nature* **487**, 94–98 (2012).
26. R. M. Merrill, B. Van Schooten, J. A. Scott, C. D. Jiggins, Pervasive genetic associations between traits causing reproductive isolation in *Heliconius* butterflies. *Proc. Biol. Sci.* **278**, 511–518 (2011).
27. M. Rossi, A. E. Hausmann, T. J. Thurman, S. H. Montgomery, R. Papa, C. D. Jiggins, W. O. McMillan, R. M. Merrill, Visual mate preference evolution during butterfly speciation is linked to neural processing genes. *Nat. Commun.* **11**, 4763 (2020).
28. C. Pardo-Diaz, C. Salazar, S. W. Baxter, C. Merot, W. Figueiredo-Ready, M. Joron, W. O. McMillan, C. D. Jiggins, Adaptive introgression across species boundaries in *Heliconius* butterflies. *PLOS Genet.* **8**, e1002752 (2012).
29. S. H. Martin, J. W. Davey, C. D. Jiggins, Evaluating the use of ABBA-BABA statistics to locate introgressed loci. *Mol. Biol. Evol.* **32**, 244–257 (2015).
30. J. J. Lewis, R. C. Geltman, P. C. Pollak, K. E. Rondem, S. M. Van Belleghem, M. J. Hubisz, P. R. Munn, L. Zhang, C. Benson, A. Mazo-Vargas, C. G. Danko, B. A. Counterman, R. Papa, R. D. Reed, Parallel evolution of ancient, pleiotropic enhancers underlies butterfly wing pattern mimicry. *Proc. Natl. Acad. Sci. U.S.A.* **116**, 24174–24183 (2019).
31. S. H. Martin, J. W. Davey, C. Salazar, C. D. Jiggins, Recombination rate variation shapes barriers to introgression across butterfly genomes. *PLOS Biol.* **17**, e2006288 (2019).
32. S. H. Martin, S. M. Van Belleghem, Exploring Evolutionary Relationships Across the Genome Using Topology Weighting. *Genetics* **206**, 429–438 (2017).
33. M. Kirkpatrick, Sexual selection and the evolution of female choice. *Evolution* **36**, 1–12 (1982).
34. M. DeGiorgio, C. D. Huber, M. J. Hubisz, I. Hellmann, R. Nielsen, SweepFinder2: Increased sensitivity, robustness and flexibility. *Bioinformatics* **32**, 1895–1897 (2016).
35. C. Mérot, B. Frérot, E. Leppik, M. Joron, Beyond magic traits: Multimodal mating cues in *Heliconius* butterflies. *Evolution* **69**, 2891–2904 (2015).
36. J. I. Meier, R. B. Stelkens, D. A. Joyce, S. Mwaiko, N. Phiri, U. K. Schliewen, O. M. Selz, C. E. Wagner, C. Katongo, O. Seehausen, The coincidence of ecological opportunity with hybridization explains rapid adaptive radiation in Lake Mweru cichlid fishes. *Nat. Commun.* **10**, 5391 (2019).
37. Q. Helleu, C. Roux, K. G. Ross, L. Keller, Radiation and hybridization underpin the spread of the fire ant social supergene. *Proc. Natl. Acad. Sci. U.S.A.* **119**, e2201040119 (2022).
38. D. R. Laetsch, G. Bisschop, S. H. Martin, S. Aeschbacher, D. Setter, K. Lohse, Demographically explicit scans for barriers to gene flow using gIMble. *PLOS Genet.* **19**, e1010999 (2023).

39. D. A. Marques, J. I. Meier, O. Seehausen, A combinatorial view on speciation and adaptive radiation. *Trends Ecol. Evol.* **34**, 531–544 (2019).
40. J. Felsenstein, Skepticism Towards Santa Rosalia, or Why Are There so Few Kinds of Animals? *Evolution* **35**, 124–138 (1981).
41. M. E. Maan, O. Seehausen, T. G. G. Groothuis, Differential survival between visual environments supports a role of divergent sensory drive in cichlid fish speciation. *Am. Nat.* **189**, 78–85 (2017).
42. S. H. Montgomery, M. Rossi, W. O. McMillan, R. M. Merrill, Neural divergence and hybrid disruption between ecologically isolated *Heliconius* butterflies. *Proc. Natl. Acad. Sci. U.S.A.* **118**, e2015102118 (2021).
43. M. R. Kronforst, L. G. Young, L. E. Gilbert, Reinforcement of mate preference among hybridizing *Heliconius* butterflies. *J. Evol. Biol.* **20**, 278–285 (2007).
44. R. M. Merrill, K. K. Dasmahapatra, J. W. Davey, D. D. Dell’Aglia, J. J. Hanly, B. Huber, C. D. Jiggins, M. Joron, K. M. Kozak, V. Llaurens, S. H. Martin, S. H. Montgomery, J. Morris, N. J. Nadeau, A. L. Pinharanda, N. Rosser, M. J. Thompson, S. Vanjari, R. W. R. Wallbank, Q. Yu, The diversification of *Heliconius* butterflies: What have we learned in 150 years? *J. Evol. Biol.* **28**, 1417–1438 (2015).
45. M. Yamaguchi, Role of regucalcin in brain calcium signaling: Involvement in aging. *Integr. Biol. (Camb.)* **4**, 825–837 (2012).
46. M. Rossi, A. E. Hausmann, P. Alcamí, M. Moest, R. Roussou, S. M. Van Belleghem, D. S. Wright, C.-Y. Kuo, D. Lozano-Urrego, A. Maulana, L. Melo-Flórez, G. Rueda-Muñoz, S. McMahan, M. Linares, C. Osman, W. O. McMillan, C. Pardo-Díaz, C. Salazar, R. M. Merrill, Speciation Behaviour/Adaptive introgression of a visual preference gene, version v1, Zenodo (2023); <https://doi.org/10.5281/zenodo.10203687>.
47. J. Troscianko, M. Stevens, Image calibration and analysis toolbox - a free software suite for objectively measuring reflectance, colour and pattern. *Methods Ecol. Evol.* **6**, 1320–1331 (2015).
48. C. A. Schneider, W. S. Rasband, K. W. Eliceiri, NIH Image to ImageJ: 25 years of image analysis. *Nat. Methods* **9**, 671–675 (2012).
49. K. J. McCulloch, F. Yuan, Y. Zhen, M. L. Aardema, G. Smith, J. Llorente-Bousquets, P. Andolfatto, A. D. Briscoe, Sexual dimorphism and retinal mosaic diversification following the evolution of a violet receptor in butterflies. *Mol. Biol. Evol.* **34**, 2271–2284 (2017).
50. G. Zaccardi, A. Kelber, M. P. Sison-Mangus, A. D. Briscoe, Color discrimination in the red range with only one long-wavelength sensitive opsin. *J. Exp. Biol.* **209**, 1944–1955 (2006).
51. K. J. McCulloch, D. Osorio, A. D. Briscoe, Sexual dimorphism in the compound eye of *Heliconius erato*: A nymphalid butterfly with at least five spectral classes of photoreceptor. *J. Exp. Biol.* **219**, 2377–2387 (2016).
52. M. Vorobyev, D. Osorio, Receptor noise as a determinant of colour thresholds. *Proc. Biol. Sci.* **265**, 351–358 (1998).

53. A. Siddiqi, T. W. Cronin, E. R. Loew, M. Vorobyev, K. Summers, Interspecific and intraspecific views of color signals in the strawberry poison frog *Dendrobates pumilio*. *J. Exp. Biol.* **207**, 2471–2485 (2004).
54. K. J. McCulloch, A. Macias-Muñoz, A. Mortazavi, A. D. Briscoe, Multiple mechanisms of photoreceptor spectral tuning in *Heliconius* butterflies. *Mol. Biol. Evol.* **39**, msac067 (2022).
55. D. A. Elston, R. Moss, T. Boulinier, C. Arrowsmith, X. Lambin, Analysis of aggregation, a worked example: Numbers of ticks on red grouse chicks. *Parasitology* **122**, 563–569 (2001).
56. N. J. Nadeau, A. Whibley, R. T. Jones, J. W. Davey, K. K. Dasmahapatra, S. W. Baxter, M. A. Quail, M. Joron, R. H. ffrench-Constant, M. L. Blaxter, J. Mallet, C. D. Jiggins, Genomic islands of divergence in hybridizing *Heliconius* butterflies identified by large-scale targeted sequencing. *Philos. Trans. R. Soc. Lond. B Biol. Sci.* **367**, 343–353 (2012).
57. S. H. Martin, K. K. Dasmahapatra, N. J. Nadeau, C. Salazar, J. R. Walters, F. Simpson, M. Blaxter, A. Manica, J. Mallet, C. D. Jiggins, Genome-wide evidence for speciation with gene flow in *Heliconius* butterflies. *Genome Res.* **23**, 1817–1828 (2013).
58. P. Jay, A. Whibley, L. Frézal, M. Á. Rodríguez de Cara, R. W. Nowell, J. Mallet, K. K. Dasmahapatra, M. Joron, Supergene evolution triggered by the introgression of a chromosomal inversion. *Curr. Biol.* **28**, 1839–1845.e3 (2018).
59. J. W. Davey, M. Chouteau, S. L. Barker, L. Maroja, S. W. Baxter, F. Simpson, R. M. Merrill, M. Joron, J. Mallet, K. K. Dasmahapatra, C. D. Jiggins, Major improvements to the *Heliconius melpomene* genome assembly used to confirm 10 chromosome fusion events in 6 million years of butterfly evolution. *G3: Genes Genomes Genet.* **6**, 695–708 (2016).
60. H. Li, R. Durbin, Fast and accurate long-read alignment with Burrows-Wheeler transform. *Bioinformatics* **26**, 589–595 (2010).
61. A. McKenna, M. Hanna, E. Banks, A. Sivachenko, K. Cibulskis, A. Kernytsky, K. Garimella, D. Altshuler, S. Gabriel, M. Daly, M. A. DePristo, The Genome Analysis Toolkit: A MapReduce framework for analyzing next-generation DNA sequencing data. *Genome Res.* **20**, 1297–1303 (2010).
62. M. Nei, L. Jin, Variances of the average numbers of nucleotide substitutions within and between populations. *Mol. Biol. Evol.* **6**, 290–300 (1989).
63. R. R. Hudson, M. Slatkin, W. P. Maddison, Estimation of levels of gene flow from DNA sequence data. *Genetics* **132**, 583–589 (1992).
64. S. R. Browning, B. L. Browning, Rapid and accurate haplotype phasing and missing-data inference for whole-genome association studies by use of localized haplotype clustering. *Am. J. Hum. Genet.* **81**, 1084–1097 (2007).
65. O. Gascuel, BIONJ: An improved version of the NJ algorithm based on a simple model of sequence data. *Mol. Biol. Evol.* **14**, 685–695 (1997).
66. S. Guindon, J.-F. Dufayard, V. Lefort, M. Anisimova, W. Hordijk, O. Gascuel, New algorithms and methods to estimate maximum-likelihood phylogenies: Assessing the performance of PhyML 3.0. *Syst. Biol.* **59**, 307–321 (2010).

67. B. L. Browning, X. Tian, Y. Zhou, S. R. Browning, Fast two-stage phasing of large-scale sequence data. *Am. J. Hum. Genet.* **108**, 1880–1890 (2021).
68. P. Danecek, A. Auton, G. Abecasis, C. A. Albers, E. Banks, M. A. DePristo, R. E. Handsaker, G. Lunter, G. T. Marth, S. T. Sherry, G. McVean, R. Durbin; 1000 Genomes Project Analysis Group, The variant call format and VCFtools. *Bioinformatics* **27**, 2156–2158 (2011).
69. W. N. Venables, B. Ripley, *Modern Applied Statistics with S* (Springer, ed. 4, 2002).
70. M. Moest, S. M. Van Belleghem, J. E. James, C. Salazar, S. H. Martin, S. L. Barker, G. R. P. Moreira, C. Mérot, M. Joron, N. J. Nadeau, F. M. Steiner, C. D. Jiggins, Selective sweeps on novel and introgressed variation shape mimicry loci in a butterfly adaptive radiation. *PLOS Biol.* **18**, e3000597 (2020).
71. C. D. Huber, M. DeGiorgio, I. Hellmann, R. Nielsen, Detecting recent selective sweeps while controlling for mutation rate and background selection. *Mol. Ecol.* **25**, 142–156 (2016).
72. C. D. Jiggins, *The Ecology and Evolution of Heliconius Butterflies* (Oxford Univ. Press, 2017).
73. A. Pinharanda, M. Rousselle, S. H. Martin, J. J. Hanly, J. W. Davey, S. Kumar, N. Galtier, C. D. Jiggins, Sexually dimorphic gene expression and transcriptome evolution provide mixed evidence for a fast-Z effect in *Heliconius*. *J. Evol. Biol.* **32**, 194–204 (2019).
74. A. Dobin, C. A. Davis, F. Schlesinger, J. Drenkow, C. Zaleski, S. Jha, P. Batut, M. Chaisson, T. R. Gingeras, STAR: Ultrafast universal RNA-seq aligner. *Bioinformatics* **29**, 15–21 (2013).
75. H. Li, B. Handsaker, A. Wysoker, T. Fennell, J. Ruan, N. Homer, G. Marth, G. Abecasis, R. Durbin, 1000 Genome Project Data Processing Subgroup, The Sequence Alignment/Map format and SAMtools. *Bioinformatics* **25**, 2078–2079 (2009).
76. S. Anders, P. T. Pyl, W. Huber, HTSeq—A Python framework to work with high-throughput sequencing data. *Bioinformatics* **31**, 166–169 (2015).
77. M. I. Love, W. Huber, S. Anders, Moderated estimation of fold change and dispersion for RNA-seq data with DESeq2. *Genome Biol.* **15**, 550 (2014).
78. S. H. Montgomery, J. E. Mank, Inferring regulatory change from gene expression: The confounding effects of tissue scaling. *Mol. Ecol.* **25**, 5114–5128 (2016).
79. H. Li, Minimap2: Pairwise alignment for nucleotide sequences. *Bioinformatics* **34**, 3094–3100 (2018).
80. S. Kovaka, A. V. Zimin, G. M. Pertea, R. Razaghi, S. L. Salzberg, M. Pertea, Transcriptome assembly from long-read RNA-seq alignments with StringTie2. *Genome Biol.* **20**, 278 (2019).
81. J. G. Doench, N. Fusi, M. Sullender, M. Hegde, E. W. Vaimberg, K. F. Donovan, I. Smith, Z. Tothova, C. Wilen, R. Orchard, H. W. Virgin, J. Listgarten, D. E. Root, Optimized sgRNA design to maximize activity and minimize off-target effects of CRISPR-Cas9. *Nat. Biotechnol.* **34**, 184–191 (2016).

82. A. Martin, N. S. Wolcott, L. A. O'Connell, Bringing immersive science to undergraduate laboratory courses using CRISPR gene knockouts in frogs and butterflies. *J. Exp. Biol.* **223** (Suppl 1), jeb208793 (2020).
83. N. D. Meeker, S. A. Hutchinson, L. Ho, N. S. Trede, Method for isolation of PCR-ready genomic DNA from zebrafish tissues. *Biotechniques* **43**, 610–614, 612, 614 (2007).
84. D. S. Wright, A. N. Manel, M. Guachamin-Rosero, P. Chamba-Vaca, C. N. Bacquet, R. M. Merrill, Quantifying visual acuity in *Heliconius* butterflies. *Biol. Lett.* **19**, 20230476 (2023).
85. E. M. Caves, J. Troscianko, L. A. Kelley, A customizable, low-cost optomotor apparatus: A powerful tool for behaviourally measuring visual capability. *Methods Ecol. Evol.* **11**, 1319–1324 (2020).
86. S. M. Van Belleghem, R. Papa, H. Ortiz-Zuazaga, F. Hendrickx, C. D. Jiggins, W. O. McMillan, B. A. Counterman, patternize: An R package for quantifying colour pattern variation. *Methods Ecol. Evol.* **9**, 390–398 (2018).
87. J. C. Gower, A general coefficient of similarity and some of its properties. *Biometrics* **27**, 857–871 (1971).
88. C. R. Hemingson, P. F. Cowman, J. R. Hodge, D. R. Bellwood, Colour pattern divergence in reef fish species is rapid and driven by both range overlap and symmetry. *Ecol. Lett.* **22**, 190–199 (2019).
89. C. J. B. Maia, C. R. Santos, F. Schmitt, S. Socorro, Regucalcin is expressed in rat mammary gland and prostate and down-regulated by  $17\beta$ -estradiol. *Mol. Cell. Biochem.* **311**, 81–86 (2008).